

A comparison of millisecond pulsar populations between globular clusters and the Galactic field

JONGSU LEE,¹ C. Y. HUI,² J. TAKATA,³ A. K. H. KONG,⁴ PAK-HIN THOMAS TAM,⁵ KWAN-LOK LI,⁶ AND K. S. CHENG⁷

¹*Department of Astronomy, Space Science and Geology, Chungnam National University, Daejeon 34134, Republic of Korea*

²*Department of Astronomy and Space Science, Chungnam National University, Daejeon 34134, Republic of Korea*

³*Institute of Particle Physics and Astronomy, Huazhong University of Science and Technology, People's Republic of China*

⁴*Institute of Astronomy, National Tsing Hua University, Hsinchu 30013, Taiwan*

⁵*School of Physics and Astronomy, Sun Yat-sen University, Guangzhou 510275, People's Republic Of China*

⁶*Department of Physics, National Cheng Kung University, 70101 Tainan, Taiwan*

⁷*Department of Physics, University of Hong Kong, Pokfulam Road, Hong Kong*

(Revised February 20, 2023)

Submitted to ApJ

ABSTRACT

We have performed a systematic study of the rotational, orbital and X-ray properties of millisecond pulsars (MSPs) in globular clusters (GCs) and compared their nature with those of the MSPs in the Galactic field (GF). We found that GC MSPs generally rotate slower than their counterparts in the GF. Different from the expectation of a simple recycling scenario, no evidence for the correlation between the orbital period and the rotation period can be found from the MSP binaries in GCs. There is also an indication that the surface magnetic field of GC MSPs are stronger than those in the GF. All these suggest dynamical interactions in GCs can alter the evolution of MSPs/their progenitors which can leave an imprint on their X-ray emission properties. While the MSPs in both GF and GCs have similar distributions of X-ray luminosity and hardness, our sample supports the notion that these two populations follow different relation between the X-ray luminosity and spin-down power. We discuss this in terms of both pulsar emission model and the observational bias.

Keywords: globular clusters: general — stars: binaries: general — pulsars: general — X-rays: general

1. INTRODUCTION

There is a consensus that millisecond pulsars (MSPs) are formed through the angular momentum transfer from their binary companions (Alpar et al. 1982; Radhakrishnan & Srinivasan 1982; Fabian et al. 1983). The first MSP, PSR B1937+21 was discovered by Backer et al. (1982). In comparison with the non-recycled canonical pulsars, MSPs are characterized by their fast rotation ($P \lesssim 20$ ms) and weak surface magnetic fields ($B_s \lesssim 10^9$ G). Thanks to the extensive surveys and the synergy of multiwavelength observations (see Hui 2018, for a review), the currently known MSP population has reached a size of ~ 600 .

X-ray emission of MSPs are believed to be originated from the backflow charged particles from the acceleration regions in their magnetospheres (e.g. Zhang & Cheng 2003). While the relativistic electron/positron cascades emit the non-thermal synchrotron X-rays when they gyrate along the magnetic field lines, thermal X-

ray emission can also be generated when these energetic particles follow the open magnetic field lines and deposit their energies on the stellar surface (e.g. Zavlin 2007; Bogdanov & Grindlay 2008). For the MSPs reside in the compact binaries, additional X-ray emission component can be resulted from the intrabinary shock (e.g. Huang et al. 2012; Hui et al. 2014).

According to their locations in our Galaxy, MSPs can be divided into two groups: the Galactic field (GF) population and globular cluster (GC) population. For the X-ray properties of MSPs in the GF, Lee et al. (2018) have conveyed a systematic survey. With a left-censored sample of 47 detections and 36 upper limits of their X-ray luminosities L_x , an empirical relation between L_x and the spin-down power \dot{E} has found to be $L_x \simeq 10^{31.05} \left(\dot{E}/10^{35}\right)^{1.31}$ erg s⁻¹ in 2-10 keV. The inferred X-ray conversion efficiency is lower than the previous estimate in the same energy band (e.g. Possenti

et al. 2002) which was subjected to selection bias with the upper-limits excluded in the previous works.

The X-ray properties of different types of MSPs in the GF have also been compared by Lee et al. (2018). The X-ray emission from the redbacks (RBs), which are characterized by their tight orbits with orbital period $P_b \lesssim 1$ day and their non-degenerate late-type companions (see Hui & Li 2019, for an updated review), are found to be generally harder and more luminous than the other classes. This can be accounted for by the contribution of their intrabinary shocks in the X-ray production (see discussion in Lee et al. 2018).

For the progenitors of MSPs, namely the low-mass X-ray binaries (LMXBs), their formation rate per unit mass in GCs is known to be orders of magnitudes higher than that in the GF (Katz et al. 1975; Clark 1975). This can be attributed to the frequent dynamical interactions in the central regions of GCs (Hui et al. 2010; Turk & Lorimer 2013). In some GCs, the stellar density can be high enough that multiple interactions of the binaries can occur (Verbunt & Freire 2014). With such complications, the evolution of compact binaries in GCs can possibly be different from those in the GF. And hence, it is not unreasonable to speculate that the characteristics of the MSPs, including the rotational, orbital and X-ray properties, in these two populations can be different.

Thanks to the sub-arcsecond angular resolution of *Chandra* X-ray Observatory, X-ray point sources can be resolved from the dense cores of GCs (e.g. Heinke et al. 2005; Bhattacharya et al. 2017; Bahramian et al. 2020; Oh et al. 2020). This enables us to identify the X-ray counterparts of MSPs by matching their radio timing positions with the X-ray source positions. With this sample, we can compare the X-ray properties of GC MSPs with their counterparts in the GF.

In this study, we first collected the updated samples of both X-ray and radio selected GC MSPs and normalized their X-ray properties. These allow us to convey a systematic analysis and compare their properties with those in the GF for investigating if there is any difference between these two populations of MSPs.

2. DATA COLLECTION AND NORMALIZATION

To be consistent with Lee et al. (2018), we define MSPs as the pulsars with rotational period $P < 20$ ms in this work. With this criterion, a sample of 204 radio selected GC MSPs are collected from the online catalogue compiled by P. Freire.¹ On the other hand, we obtained an updated radio selected sample of 386 MSPs

in the GF from the online catalogue maintained by West Virginia University.² The rotation period P and the orbital period P_b of the MSPs are also collected from these two catalogues. For obtaining the reliable estimates of spin-down rate \dot{P} from a sub-sample of GC MSPs, please refer to Section 4.

To identify the X-ray counterparts of GC MSPs, we consider the sources detected by the Advanced CCD Imaging Spectrometer (ACIS) onboard *Chandra*. With its sub-arcsecond spatial resolution, ACIS enables the X-ray counterparts to be resolved from the crowded environment in GCs and provide their temporal and spectral information. The information of ACIS observations of MSP-hosting GCs are summarized in Table 1.

We found that 56 GC MSPs have their X-ray counterparts previously reported in the literature. Their properties and the relevant literature are summarized in Table 2. In order to compare the X-ray properties of GF MSPs reported by Lee et al. (2018), we have to normalize the data with the same procedures adopted in their study. In the following, we describe the strategy for collecting the X-ray parameters in this work.

If a source has its X-ray spectrum characterized by an absorbed power-law (PL) model and with the spectral parameters reported in the existing literature, we adopt these reported properties in our work. However, since different studies have adopted different energy ranges in their X-ray analyses, it is necessary to normalize our X-ray fluxes of GC MSPs in the same energy band.

With the aid of PIMMS, we computed the absorption-corrected X-ray fluxes f_x by integrating the spectral model in two energy ranges: 0.3-8 keV and 2-10 keV. While 0.3-8 keV is a standard band for analysing *Chandra* ACIS data, f_x in 2-10 keV allow us to compare with those of GF MSPs reported by Lee et al. (2018). Using the distances of the GCs d (see Table 2), we computed the X-ray luminosities as $L_x = 4\pi d^2 f_x$.

This method allows us to obtain L_x and the effective X-ray photon indices Γ for the X-ray emitting MSPs in M13, M62, NGC 6397, Terzan5, and M22. Their parameters and the corresponding references are given in Table 2.

For the sources that do not fulfill the criteria above, we analyzed the data directly by using CIAO (v.4.12). All the data were firstly reprocessed by using the `chandra_repro` script with updated calibration (CALDB v.4.9.2.1) and was filtered in the 0.3-8 keV energy band using `dmcopy` task. All the data were reprocessed with subpixel event repositioning in order to

¹ <http://www.naic.edu/~pfreire/GCpsr.html>

² <http://astro.phys.wvu.edu/GalacticMSPs/GalacticMSPs.txt>

facilitate a high angular resolution analysis. For the GCs with more than one observation, we first combined the data at different epochs by the `merge_obs` script. The images were subsequently produced with a binning factor of 0.5. By running a wavelet detection algorithm (`wavdetect`) on the merged images with a range of scales (1.0, 1.414, 2.0, 2.828, 4.0), X-ray counterparts of the GC MSPs were identified if the sources were detected at a significance larger than 3σ at the radio timing positions.

The X-ray spectra of these counterparts were extracted by using `specextract` in each individual observation. All the response files were generated by the same tool. The source extraction regions were selected so as to minimize the contamination of nearby sources. And the background regions were sampled in the circular source-free regions around the GCs with the radii in a range of 10-20 arcsec. All the spectral fittings in this work were performed in 0.3-8 keV with XSPEC (v.12.9). In view of low-counts data for most of the cases, all the analyses were performed with Cash statistics (Cash 1979), which enables us to perform fitting with unbinned data (cf. Eq. 7 in Cash 1979). This should give us less biased results than the binned analysis. If a source has been observed more than once (see Table 1), its spectra obtained from different observations were simultaneously fitted so as to obtain tighter constraints on its X-ray properties.

In order to better constrain the spectral parameters and hence the X-ray fluxes, we took the column absorption N_H as a fixed parameter throughout our analysis. If N_H has been reported in the literature, the value is adopted for spectral fitting and computing the absorption-corrected flux. Otherwise, N_H were estimated from the optical extinction $E(B - V)$ of the GCs (Harris 1996) through the correlation between these two quantities (Güver & Özel 2009).

All the spectra were fitted with a simple absorbed PL model with XSPEC (i.e. `TBABS × POWERLAW`). With the multiplicative component `CFLUX` (`TBABS×CFLUX×POWERLAW`), we obtained a robust estimate of the unabsorbed flux as well as its 1σ uncertainty in both 0.3-8 keV and 2-10 keV energy bands.

With the aforementioned procedures, we have identified 56 confirmed X-ray detections of MSPs in 12 GCs and obtained the normalized estimates of their L_x and Γ (Table 2). The sample size is comparable with the X-ray selected MSPs found in the GF (Tab. 1 in Lee et al. 2018). The updated statistics of these radio and X-ray selected MSPs in different GCs are shown in the upper panel of Figure 1. Following Lee et al. (2018), we divided the MSPs into four different classes, isolated (Iso), red-back (RB), black widow (BW) and non-“spider” binaries

(Oth). Their corresponding fractions of the radio/X-ray selected samples in the GF and GCs are shown in the lower panel of Figure 1.

Among our X-ray selected MSPs in 12 GCs, the samples in 7 GCs (i.e. M4, M13, M62, NGC 6397, Terzan5, M28, and M22) have also been covered by the catalogue compiled by Bahramian et al. (2020). This allows us to cross-check the validity of our results. Within the tolerance of the statistical uncertainties, our estimates are found to be consistent with those given in Bahramian et al. (2020).

We found that 60 additional GC MSPs with known radio timing positions have been covered by the archival *Chandra* ACIS data serendipitously. This enables us to also search for their X-ray counterparts. Using the same procedures of data reduction and source detection described above, we did not find any additional X-ray emitting GC MSPs with detection significance larger than 3σ in the merged images.

Despite the non-detections, the archival data still allow us to constrain the limiting L_x of these 60 GC MSPs. In examining the $L_x - \dot{E}$ relation for the MSPs in the GF, Lee et al. (2018) have shown that a less biased relation can be obtained from a survival analysis with the upper-limits of L_x included (see Section 4). To obtain the 1σ limiting fluxes, we assumed a simple PL model with $\Gamma=2$ and N_H adopted from the literature or inferred from the $E(B - V)$ of the corresponding GC. Together with the distances towards these GCs, we placed 1σ limiting luminosities of these additional 60 GC MSPs in 0.3–8 keV and 2 – 10 keV. The results are summarized in Table 3.

3. VARIABILITY ANALYSIS

Apart from the periodic variations across the orbit resulted from different causes (e.g. intrabinary shock, eclipse of emission region, heating of companion surface), secular changes can also occur in a pulsar. The discoveries of RBs show that the properties of MSPs can vary considerably in different wavelengths as they switch between rotation-powered state and accretion-powered state (e.g. Papitto et al. 2013a; Takata et al. 2014). On the other hand, evidence of variable X-ray/ γ -ray emission have also been observed from some isolated pulsars in GF (e.g. Lin et al. 2021; Takata et al. 2020; Hermsen et al. 2013).

All these indicate that emission from a pulsar might not be as stable as previously thought. Since a number of GC MSPs in our sample have been observed by *Chandra* more than once, we are able to characterize their X-ray variabilities.

Bahramian et al. (2020) have included the results of variability test (i.e. p -values for Kolmogorov-Smirnov

(K-S) test) for 7 out of 12 GCs in our sample. Among all 56 X-ray counterparts of GC MSPs in Table 2, 6 sources have p -values < 0.05 for the K-S test as reported in Bahramian et al. (2020) (M62 B, NGC6397 A, M28 A, M28 I, M28 L and Terzan5 P). This indicates the possible variable X-ray emission from these sources.

Our variability analysis was divided into two parts: (1) long-term variability search and (2) short-term variability search. For (1), we searched for the possible X-ray flux variations of the targets among observations in different epochs. For (2), we searched for the possible variability within a single observation.

For the long-term variability analysis, we only consider the observations in which the X-ray counterparts are detected with a significance $> 3\sigma$ in a single exposure. In order to compare the f_x of a given target in different epochs, we fitted its X-ray spectra obtained from individual observations. The response files generated in each observations can account for the possible instrumental variation among them. By fitting a simple absorbed PL model (with N_H fixed) for each spectra, we obtained the estimates of absorption-corrected f_x of a source in different epochs. Using these estimates, we constructed the long-term background-subtracted X-ray light curves for the subsequent analysis.

In order to identify the candidates that demonstrated long-term X-ray variability, we employed the Bayesian block algorithm that generates the optimal adaptive-width blocks (Scargle et al. 2013). Even if the sequential data is not evenly sampled, the block-wise representation generated by this method can help to indicate local variability (e.g. Ahnen et al. 2016). Using the routine `modeling.bayesian.blocks.bayesian.blocks` in the python library HEPSTATS, we have identified 10 sources require more than one block in modeling their long-term X-ray light curves. These are 47Tuc E, 47Tuc W, NGC6397 A, NGC6752 F, M28 A, M28 I, M28 L, Terzan5 A, Terzan5 P and Terzan5 ad.

To scrutinize the significance of these variability candidates, we used two-sample Kuiper test (Stephens 1970) to compare their light curves with the uniform distributions determined by their corresponding mean fluxes. For this analysis, we utilized the routine `kuiper.twoside` in ASTROPY package (v.5.1). In this work, we consider a source has possible long-term X-ray variability if the p -value inferred from Kuiper test is < 0.05 . We found that only two sources from the short-list obtained from the Bayesian block analysis, M28 I and NGC6752 F, fulfill this criterion. Their long-term X-ray light curves are shown in Figure 2 with the identified Bayesian blocks illustrated. In the followings, we describe their temporal behaviors in further details.

M28 I (IGR J18245-2452), which is a RB has been found to swing between accretion-powered state and rotation-powered state (Papitto et al. 2013a), is the most significantly variable X-ray source in our sample ($p \sim 6.8 \times 10^{-24}$). This is consistent with the results reported by Linares et al. (2014) which has presented a detailed analysis of this source.

The X-ray counterpart of the isolated MSP NGC6752 F can be detected in 6 out of 7 archival *Chandra* observations. The non-detection in the observation on 2017 July 25 (MJD 57959.83) can be ascribed to its relatively short exposure time (~ 18 ks). For this epoch, we placed a 1σ limiting L_x of 3.9×10^{30} erg/s and 1.9×10^{30} erg/s in 0.3-8 keV and 2-10 keV respectively. In most of these observations, NGC6752 F behaves as a steady X-ray source except for the recent observation in 2017. In this epoch, its L_x is found to increase by a factor of ~ 5 in comparison with its previous level (Figure 2). Kuiper test gives a p -value of 0.011 and suggests the variability can be significant. We further investigated whether such X-ray flux variation can be contaminated by the nearby bright sources. One MSP (NGC6752 D) and two cataclysmic variables (CVs) (CX 1 & CX 5 in Forestell et al. 2014) are bright sources located at $\sim 4.6''$, $\sim 7.4''$, and $\sim 6.5''$ away from NGC6752 F respectively. There is no evidence of long-term X-ray variation found for NGC6752 D. Moreover, we do not find any resemblance between the long-term X-ray variation of NGC6752 F and its nearby CVs. Therefore, we concluded that the long-term X-ray variation of NGC6752 F is unlikely a result from the contamination of these bright sources.

We have also searched for the possible short-term variability within each observation windows by utilizing Gregory-Loredo variability algorithm (Gregory & Loredo 1992) for computing the odd ratios that the arrival times are not uniformly distributed in time. The algorithm is implemented in the CIAO tool `glvary` which assigns a variability index according to the odd ratios. In this work, we set the criterion that a source demonstrates variability within a single observation if the inferred variability index is larger than 6. This implies the probability of this source to be variable is $\gtrsim 90\%$. For avoiding the false alarm which results from the fluctuation due to low count statistics, we only consider the cases with more than 50 counts.

Using the unbinned event lists and the corresponding effective areas, we have identified 3 GC MSPs, M28 I, NGC6397 A and Terzan5 P, which satisfy the aforementioned criterion in 6 observations. Their background-subtracted light curves are shown in Figure 3. The bin-

ning of these light curves were determined by `glvary` which give rise to the optimal variability.

Short-term X-ray variability of M28 I can be found in 3 observations of this cluster (Obs.ID: 9132, 9133 and 14616). All these observations were performed when M28 I were in the accretion-powered state. Its light curves on 2008 August 7 (Obs.ID: 9132) and 2008 August 10 (Obs.ID: 9133) show that the system was switching abruptly between the low state (with count rate of 0.02 count/s in 2-10 keV) and the high state (> 0.02 count/s in 2-10 keV). These are consistent with the findings reported by [Linares et al. \(2014\)](#) which suggest this can be originated from the change of the magnetospheric radius due to the fluctuation of accretion flow. On the other hand, its light curve on 2013 April 28 (Obs.ID: 14616) also shows variable X-ray variation though it was less dramatic as the other two epochs. We note that this observation was close to the end of the thermonuclear outburst ([Linares et al. 2014](#)) and just less than five days before it was found to switch back to rotation-powered state ([Papitto et al. 2013b](#)).

For the RBs Terzan5 P and NGC6397 A, their X-ray flux variation can be originated from the intrabinary shocks. Short-term X-ray variability of NGC6397 A can be identified in a single observation on 2007 June 22 (Obs. ID: 7461). This observation started around the epoch when the pulsar was in superior conjunction (i.e. when the companion was located between the neutron star and the observer). The X-ray flux of the system began to rise gradually when the system was moving away from this phase. This is consistent with the findings reported by [Bogdanov et al. \(2010\)](#). A significant orbital X-ray modulation of Terzan5 P has been reported by [Bogdanov et al. \(2021\)](#) recently. Among all 18 *Chandra* ACIS observations of Terzan 5, short-term variability can be found in two observations on 2011 April 29 (Obs. ID: 13252) and 2011 September 8 (Obs. ID: 14339), which might be resulted from the fluctuations of the interactions between the pulsar wind and the stellar wind from the companion.

We noted that the orbital variabilities of Terzan5 O, Terzan5 ad and M28 H were reported by [Bogdanov et al. \(2021, 2011\)](#), in which all the data were folded to their orbital periods. This is different from the scope of searching short-term variabilities within a single observation window in our current work. For these MSPs, their net counts are all less than 50 in all individual observations. Since they are lower than our predefined criterion for avoiding false alarm, they were not considered in our short-term variability search.

4. CORRELATION & REGRESSION ANALYSIS

The spin-down power \dot{E} of a pulsar is derived from P and \dot{P} , $\dot{E} = 4\pi^2 I \dot{P} P^{-3}$, where P , \dot{P} , and I are the rotational period, period derivative and the moment of inertia, respectively. In examining GF MSPs, [Lee et al. \(2018\)](#) have found a $L_x - \dot{E}$ relation of $L_x \simeq 10^{31.05} \left(\dot{E}/10^{35}\right)^{1.31}$ erg s $^{-1}$ in 2-10 keV. It will be instructive if one can construct a corresponding relation of the GC MSPs for comparison. Different from the GF MSPs, the MSPs in a GC are affected by the acceleration due to the cluster's gravitational potential. Hence, the Doppler effect can bias the measurements of \dot{P} (e.g. [Toscano et al. 1999](#)). A large number of GC MSPs are found to have negative \dot{P} (cf. [Cheng & Taam 2003](#)). This can complicate the estimation of the derived parameters such as \dot{E} and surface magnetic field strength which is estimated as $B_s \simeq \sqrt{\frac{3c^2 I}{2\pi^2 R_{NS}^6} \dot{P} P}$, where c is the speed of light and R_{NS} is the radius of the neutron star which is assumed to be 10 km throughout this work.

[Bogdanov et al. \(2006\)](#) have adopted a King model to compute the cluster acceleration term for each MSP in 47 Tuc, and \dot{E} are calculated by the intrinsic \dot{P} which have the acceleration terms subtracted. Using these estimates, the authors examined the $L_x - \dot{E}$ relation in 47 Tuc and obtained $L_x \propto \dot{E}^{0.24 \pm 1.1}$. However, in examining the correlation between L_x and \dot{E} in their adopted sample by the Spearman rank correlation test, we found the correlation is very weak (p -value ~ 0.4). The large uncertainties of their best-fitted $L_x - \dot{E}$ relation can be ascribed to this. While a King model provides a statistically reasonable model for the acceleration profile of a GC ([King 1962](#); [Prager et al. 2017](#)), a small sample in this case can be hampered by the systematic uncertainties.

For the GC MSPs in the binaries, long-term radio timing can provide another way for uplifting the contamination by their acceleration. [Freire et al. \(2017\)](#) have measured the time derivatives of orbital period $\dot{P}_{b,obs}$ of 6 MSPs in 47 Tuc. Intrinsic \dot{P}_{int} can be estimated by $\dot{P}_{int} = \dot{P}_{obs} - \frac{\dot{P}_{b,obs}}{P_b} P$. On the other hand, [Prager et al. \(2017\)](#) have also measured the \dot{P}_b for 9 MSPs in Terzan 5 as well as 47Tuc J which enable one to estimate their \dot{P}_{int} .

These studies of long-term radio-timing allow us to form a left-censored sub-sample of 16 MSPs with reliable estimates of \dot{E} (12 X-ray detections + 4 upper-limits of L_x). Hereafter, we refer this sub-sample as Group A. Their \dot{P}_{int} as well as the derived \dot{E} and B_s are summarized in [Table 4](#).

Applying the Spearman rank test on the $L_x - \dot{E}$ relation on Group A, we obtain p -values of 0.013 and 7×10^{-3} for L_x in 0.3-8 keV and 2-10 keV respectively

(Table 5). These suggest a much more significant correlation than the sample adopted by Bogdanov et al. (2006).

We have also examined the correlation with a larger data set by appending Group A with those have their King model corrected \dot{P} reported in the literature. This can enlarge the sample size to 24 GC MSPs (20 confirmed X-ray detections and 4 upper-limits of L_x , see Table 4). We refer this sample as Group B hereafter. Spearman rank test on this group yields p -values of 10^{-3} and 2×10^{-4} for $L_x - \dot{E}$ in 0.3-8 keV and 2-10 keV respectively (Table 5). Comparing with Group A, the improved significance of Group B is due to the enlarged sample.

On the other hand, the \dot{P} of M28 A ($\dot{P} = 1.62 \times 10^{-18}$) is larger than those of the other GC MSPs by orders of magnitude. It is reasonable to argue that the effect of cluster acceleration on its \dot{P} is not significant. Therefore, we further expanded Group B by including M28 A and we refer this sample as Group C hereafter. Spearman rank test on this group yields p -values of 2×10^{-4} and 4×10^{-5} for $L_x - \dot{E}$ in 0.3-8 keV and 2-10 keV respectively (Table 5) which indicate significant correlation between these two parameters.

Apart from the improvement of the correlation, the uncertainties of \dot{P} and hence \dot{E} in our adopted sample are also reduced. The averaged percentage error of \dot{P} for the 47 Tuc MSPs, as given by Freire et al. (2017) based on long-term pulsar timing, is $\sim 65\%$. This is smaller than that in the sample adopted by Bogdanov et al. (2006) (i.e. $\sim 75\%$). For the sample from Terzan 5, Prager et al. (2017) do not provide any error estimates for their \dot{P} . Since they are also obtained through long-term timing, we assumed the average percentage errors of the samples in Prager et al. (2017) are comparable with that in Freire et al. (2017) and computed the uncertainties accordingly. Combining with the other King model corrected \dot{P} , the overall averaged percentage error in Group B is found to be 68%. With M28 A included, the overall averaged percentage error in Group C becomes 65%.

The stronger correlation and the reduced uncertainties in our current sample prompt us to re-examine the $L_x - \dot{E}$ relation for GC MSPs and compare with their counterparts in the GF. In this work, all the regression analyses were performed in the framework of Bayesian inference. Instead of giving the point estimates, the posterior distributions of the parameters are reported so as to alleviate biases resulted from the small sample size. We adopt the R-package LIRA (Sereno 2016) for our analyses, which not only allows an ordinary linear regression but also enables a survival regression anal-

ysis with the upper-limits of L_x taken into account. In Bayesian framework, the conditional probability of a measurement x with the given model X is denoted by $P(x|X)$. In our analysis, $P(x|X)$ is proportional to a Gaussian for the detections. For the case that the observational results are expressed as upper limits, the conditional probability is truncated by a Heaviside function $H(x - x_{ul})$ where x_{ul} is the upper limit for the left-censored data points (cf. Appendix in Willis et al. 2021). These treatments of the upper-limits are implemented in LIRA. This can result in a less biased estimate for the $L_x - \dot{E}$ relation.

For the linear regression with a form of $\log L_x = \alpha \log \dot{E} + \beta$, the measurement uncertainties in both independent and dependent variables are taken into account. We assume a Student t -distribution and an uniform distribution as the priors for α and β respectively. A 2D posterior probability distribution of these parameters was inferred through Markov chain Monte Carlo (MCMC). We have used four parallel chains with 2×10^6 iterations on each. The first 1% of the samples from each chain were set as the initial burn-in. With these adaptation iterations excluded, all the other samples are used to approximate the posterior probability distribution.

Since our aim is to compare $L_x - \dot{E}$ relation between the MSPs in GC and GF, we analysed the data in both populations with the same procedures as aforementioned. For GC MSPs, we have started with the complete censored sample of Group C (i.e. with upper-limits of L_x taken into account) as given in Table 4. For GF MSPs, we adopted the censored samples given by the Tables 1 and 2 in Lee et al. (2018).

The comparisons of the marginalized posterior distributions of α and β inferred from Group C and the GF population are shown in Figure 4. For GF MSPs, the distribution of the slope (i.e. α) is found to be peaked around ~ 0.9 and ~ 1.2 in 0.3-8 keV and 2-10 keV respectively. The latter one is consistent with the point estimate reported by Lee et al. (2018) in the same energy band. On the other hand, the posterior distribution of α inferred from the GC MSPs in Group C is peaked around ~ 0.6 and ~ 0.8 in 0.3-8 keV and 2-10 keV respectively. The comparison of the $L_x - \dot{E}$ relation in these two populations suggests a possible difference.

The plots the $L_x - \dot{E}$ relations in Figure 4 are shown for a further comparison. Uncertainties estimated from the ranges centered at the peaks and bracket 68% of the samples in the marginalized posterior distributions are illustrated as the shaded regions in these plots. The difference between these two populations is also suggested by the lack of overlap between their shaded regions.

By visually examining the plots of $L_x - \dot{E}$ for the GC MSPs in Figure 4, the asymmetric distribution of the data points above and below the best-fit relation suggests the fitting is far from desirable. We speculate that M28 A can possibly be an outlier. Since the regression analysis is weighed by the reciprocal of the uncertainties of the data, the fact that the errors of \dot{E} and L_x of M28 A is much smaller than those of the other GC MSPs can result in a strong bias towards this single data point.

To quantify this issue, we have computed the interquartile range (IQR) of $\log L_x$. For detecting outliers, we adopted the conventional criterion of 1.5 times of IQR, which is found to be $\log L_x = 29.96 - 31.72$ (0.3-8 keV) and $\log L_x = 28.92 - 31.61$ (2-10 keV) in Group C. With this procedure, M28 A is the only source lies outside $1.5 \times \text{IQR}$ of Group C.

Distinctions between M28 A and the majority of GC MSPs can also be discussed in terms of physical reasons. First, its characteristic age ($\tau \sim 3 \times 10^7$ yrs) is much smaller than the other MSPs. Apart from its high value of L_x , the X-ray pulses of this isolated MSP have a very narrow profile which suggests its non-thermal nature with the origin from the magnetospheric accelerator (Du et al. 2015). Also, its X-ray emission can be detected at energies up to ~ 50 keV. All these make the X-ray properties of M28 A very different from the thermal X-rays originated from most of the isolated MSPs in GCs. Furthermore, it is one of the two MSPs which have glitches detected so far (Cognard & Backer 2004; McKee et al. 2016). This might suggest M28 A is more similar to young energetic pulsars than a typical MSP.

To be consistent, although the best-fit $L_x - \dot{E}$ relation for the GF MSPs in Figure 4 is reasonable, we have also searched for the possible outliers in the GF sample with the same procedure we applied in the GC sample. In 0.3-8 keV, PSR J0218+4232 and PSR B1937+21 are found lying outside $1.5 \times \text{IQR}$ of $\log L_x$ (28.79 - 32.72) of the GF sample. And in 2-10 keV, only PSR J0218+4232 lies outside the corresponding range ($\log L_x = 27.32 - 33.19$). This prompts us to re-do the fitting by considering both of them as the outliers.

With the outliers removed from both GC and GF samples, we have re-run the regression analysis for inferring $L_x - \dot{E}$ relation. The results are shown in Figure 5. For the GF MSPs, excluding PSR J0218+4232 and PSR B1937+21 only results in a slightly flatter $L_x - \dot{E}$ relation in comparison with the case including all the samples (i.e. Figure 4). Their difference can be reconciled with the tolerance of their uncertainties.

On the other hand, in the case of GC MSPs, the posterior distribution of α inferred with M28 A removed

(i.e. Group B) is peaked around ~ 0.4 and ~ 0.5 in 0.3-8 keV and 2-10 keV respectively. The relation appears to be much flatter than that shown in Figure 4. And we found that the quality of the fitting is much improved as similar number of data points are above and below the best-fit line. With the outliers excluded, the comparison between the posterior distributions of α and β suggests the difference in the $L_x - \dot{E}$ relation between GC MSPs and GF MSPs becomes more significant.

A recent study of the MSPs in Terzan 5 has suggested a positive correlation between L_x and the X-ray hardness (cf. Figure 3 in Bogdanov et al. 2021). With the effective photon index given in Table 2 as a measure of X-ray hardness of GC MSPs (i.e. smaller Γ implies harder X-ray emission), we are able to examine if this relation can be found in the full sample of X-ray selected GC MSPs with the photoelectric absorption corrected. Spearman rank test suggests a strong correlation between L_x and Γ with a p -value of 5.6×10^{-16} and 5.3×10^{-5} in both 2-10 keV and 0.3-8 keV. For the non-detections in Table 3, the upper-limits of L_x are calculated by assuming a PL model with fixed Γ and hence they are not very informative for examining the relation between L_x and Γ . Therefore, we ignored the upper limits in the regression analysis of $\log L_x - \Gamma$.

Using the procedures as described above, we obtained the marginalized posterior distributions for the parameters a and b in the assumed linear relation of $\log L_x = a\Gamma + b$. We have applied the same analysis on the GF sample as given by Lee et al. (2018). The comparison of this relation between these two populations are shown in Figure 6. No significant difference in terms of X-ray luminosity and hardness is found between the MSPs in GCs and GF.

From the literature, we have also obtained the information of whether the X-rays from the GC MSPs are dominated by thermal or non-thermal emission which are summarized in Table 2. In Figure 6, we differentiate the non-thermal dominant and thermal dominant cases by different symbols. We found that the non-thermal dominant X-ray GC MSPs are characterized with an effective photon index of $\Gamma < 2$ in our analysis. On the other hand, the thermal X-ray emitters are generally characterized with $\Gamma > 2$. The fact that the non-thermal dominant X-ray GC MSPs are generally more luminous can be due to the presence of additional harder X-ray components from the intrabinary shock in these systems (Lee et al. 2018).

Many studies have shown that the final state of a MSP strongly depends on the initial mass of its companion and the orbital separation (e.g. Tauris 2011; Liu & Chen 2011). Furthermore, evolutionary status of the compan-

ion at the onset of the Roche lobe overflow (RLO) is suggested to be a key factor in determining the timescale of the mass transfer phase which can directly affect the nature of the MSP (Tauris 2011; Tauris & Savonije 1999). The longer the mass transfer phase (i.e. more mass accreted by the neutron star) will result in a faster rotating MSP (cf. Fig. 5 in Liu & Chen 2011).

If the orbital separation of the progenitor is wider, the companion needs to be more evolved by the time it fills its Roche lobe and transfers its mass to the neutron star. This will lead to a shorter mass transfer phase and hence a relatively slower rotating MSP. Hence, This suggests that investigating the correlation between P_b and P (i.e. Corbet diagram) can provide a fossil record for the evolutionary history of compact binaries.

The distributions of P vs P_b for radio/X-ray selected samples in GF and GCs are shown in Figure 7. We started the analysis with all the MSP binaries. With Spearman rank test, we found that P and P_b in radio selected sample of GF MSPs are strongly correlated (p -value $\sim 7 \times 10^{-9}$). On the other hand, the correlation becomes weaker in their X-ray selected sample and it is marginally significant (p -value ~ 0.06), which can be due to the much reduced sample size of the X-ray emitting GF MSPs.

However, in both radio selected and X-ray selected samples of GC MSPs, we do not find any evidence for the correlation between P and P_b (p -value > 0.1 in both cases). The comparisons of P - P_b correlation test for the MSPs in GF and GCs are summarized in Table 6. The lack of such correlation in GC MSPs is likely a results of dynamical interactions (see the discussion in Section 6).

For the GF MSPs, we further examined P - P_b correlation from each types of MSP binaries. In Figure 7, the binaries with different nature of companion are represented by different symbols. By running the Spearman rank correlation test on each types of MSP binaries, we found that only those with a helium white dwarf (He WD) as the companion show a significant correlation between P and P_b (p -value = 7.0×10^{-4}). This can be accounted by the relatively simple evolutionary track with wide LMXBs as progenitors (Case B RLO Tauris 2011). For the other types of MSP binaries (e.g. spider MSPs, MSPs with CO WD companion), the lack of P - P_b correlation might be a result of the more complex evolutionary channels for their formation (Tauris & Savonije 1999; Tauris 2011).

The P - P_b correlation found in radio selected GF MSPs leads us to perform the Bayesian regression analysis by assuming a linear relation of $\log P = m \log P_b + c$. We have run the analysis for the cases with the full sam-

ple as well as only with those have a He WD companion. The marginalized posterior probability distributions of m and c as well as the best-fit relation are shown in Figure 7.

5. GLOBULAR CLUSTER MSPS VS. GALACTIC FIELD MSPS

To investigate whether the frequent stellar interactions in GCs have any effects on the physical properties of their MSPs, we compare a set of parameters of GC MSPs with those of their counterparts in the GF through standard statistical tests. Six parameters, including Γ , L_x^{2-10} , P_b , P , B_s and \dot{E} , are chosen in this analysis.

Before any comparison, we first constructed the unbinned empirical cumulative distribution functions (eCDFs) for each parameter (Figure 8-10). To quantify the difference between any two eCDFs in consideration, we employed two different non-parametric statistical tests: two-sample Anderson-Darling (A-D) test and Kolmogorov-Smirnov (K-S) test. While K-S test is widely used in literature, we notice it has several drawbacks.³ For example, it is not sensitive to supremum distance between two eCDFs far away from their centers. On the other hand, two-sample A-D test provides a more sensitive method in identifying the difference between two distributions. p -values inferred from both A-D and K-S tests in different comparisons are listed in Table 7 and 8. In this study, if the p -value inferred from either test is $\lesssim 0.05$, the difference between the eCDFs is considered to be plausible and will be further discussed.

We first compared the X-ray luminosities and hardness between the MSPs in GF and GCs. The eCDFs of L_x^{2-10} and Γ for all known X-ray emitting MSPs in these two populations are shown in Figure 8. While we do not find any significant difference in Γ between the X-ray selected samples in GF and GCs (p -value > 0.1 in both A-D and K-S test), A-D test suggests a marginal difference in L_x^{2-10} (p -value ~ 0.02). In examining their eCDFs, the possible difference can be in the low luminosity range of $L_x^{2-10} \lesssim 5 \times 10^{29}$ erg/s. This can be due to the fact that there are more nearby systems in the GF which allow fainter MSPs to be detected.

We have also divided the full sample of X-ray selected MSPs into four classes (Iso, RB, BW and Oth) and compared the corresponding classes in GCs and GF (e.g. RBs in GCs vs RBs in GF). The results are shown in Figure 9 and Table 7. We found the p -values inferred

³ <https://asaip.psu.edu/articles/beware-the-kolmogorov-smirnov-test/>

from both tests are > 0.05 for all cases and hence no significant difference in the X-properties between the corresponding classes in GCs and GF can be identified with the current sample.

For comparing P_b , P , B_s and \dot{E} , we have examined both radio selected and X-ray selected samples in order to investigate the possible selection effect imposed by X-ray observations. For the comparison of B_s and \dot{E} , we started with the outliers in both populations (i.e. M28 A, PSR J0128+4232 and PSR B1937+21) excluded.

We found that all these four parameters are significantly different between the radio selected MSPs in GCs and GF (see the first row of Figure 10). The most obvious differences are found between their P_b and \dot{E} , in which A-D test gives p -values of $\sim 10^{-5}$ and 10^{-4} respectively (see Table 8).

However, when we compare the X-ray selected samples of these two populations, the differences in their P_b and \dot{E} distributions disappear (see the second row of Figure 10). For example, the significance for the differences between their P_b and \dot{E} drop drastically (p -value ~ 0.7 from A-D test, see Table 8). This clearly indicates the presence of selection effect imposed by X-ray detections.

To further examine such effect, we tabulate the medians of these four parameters of both X-ray selected and radio selected samples in GF and GCs (see Table 9). We have also compared the X-ray/radio selected eCDFs in GF and GCs, which are shown in the third and the fourth rows in Figure 10 respectively.

In view of the large uncertainties of B_s and \dot{E} for the GC MSPs, we examined the possible impact of the measurement errors on the aforementioned inference by Monte Carlo sampling. We assumed a Gaussian distribution centered on each of the observed values of $\log B_s$ and $\log \dot{E}$ in Table 4 with the corresponding errors as the standard deviations. A set of simulated sample can then be randomly drawn from each of these distributions. In total, 10000 sets of simulated samples were generated in our experiment. For each set of sample, we have run A-D test to compare its eCDFs with those of GF MSPs and computed the corresponding p -values.

In Figure 11, we show the empirical distributions of p -values obtained from the aforementioned Monte Carlo method. The green dashed lines illustrated the p -values computed with the observed data (cf. Table 8). Taking $p < 0.05$ as the benchmark for two distributions being different, we estimated the probabilities of obtaining $p < 0.05$ from these empirical distributions. For comparing \dot{E} between the radio selected MSPs, 100% of our simulated data result in $p < 0.05$.

On the contrary, none of the simulated data leads to $p < 0.05$ in comparing \dot{E} between the X-ray selected MSPs. These results support our assertion that \dot{E} of the MSPs in GC and GF are different in the radio selected samples but such difference is diminished in the X-ray selected samples. For comparing B_s between the MSPs between GCs and GF, we found that $\sim 99\%$ and $\sim 96\%$ of the simulated data give p -value below the benchmark in comparing the radio selected and X-ray selected samples respectively. These support the conclusion that the distributions of B_s for the MSPs in GCs and GF are different, regardless of X-ray selected or radio selected.

We have repeated the analysis of comparing B_s and \dot{E} between the MSPs in GCs and GF with the outliers included. The comparisons of eCDFs and the empirical distributions of p -values obtained from the Monte Carlo method are shown in Figure 12 and Figure 13 respectively. We found that the results are fully consistent with those inferred from the analysis with the outliers removed. In Figure 13, while 100% of our simulated data result in $p < 0.05$ for the comparison of \dot{E} between the radio selected MSPs in GCs and GF, there is only 0.1% of simulated data below this benchmark in comparing the same parameter between the X-ray selected MSPs in these two populations. On the other hand, in comparing B_s between the MSPs between GCs and GF, we found that 100% and 98% of the simulated data show $p < 0.05$ in the radio selected and X-ray selected MSPs respectively.

For the GF MSPs, both P_b and P in their X-ray selected sample are significantly shorter than those in their radio selected sample (Table 9). A-D test yields the p -values of $\sim 10^{-3}$ in comparing the corresponding eCDFs which indicates such differences are significant (see the third row of Figure 10 and Table 8). On the other hand, we found that the surface magnetic field strength B_s of both radio selected and X-ray selected GF MSPs are very similar (Figure 10 and Table 8). Since \dot{E} scales as $\dot{E} \propto B_s^2 P^{-4}$, the difference of this parameter between the radio selected and X-ray selected GF MSPs is expected as A-D test yields a p -value of $\sim 10^{-4}$.

It is clear that the X-ray observations have detected MSPs in the GF with faster rotation (i.e. small P) and hence more powerful (i.e. higher \dot{E}) (see Table 9).

For the X-ray emitting GC MSPs, however, we do not find any significant selection effect imposed by X-ray observations in the GC MSP population (see Table 9, Figure 10/Figure 12). For all four parameters considered in this analysis (see the fourth row of Figure 10/Figure 12), neither A-D test nor K-S test can identify any significant difference between the radio selected and X-ray selected samples in GC MSPs (see Table 8). For example, differ-

ent from the case of GF MSPs, the X-ray selected MSPs in GCs do not appear to rotate significantly faster than their radio selected sample ($p \sim 0.13$ by A-D test).

There is another interesting feature found in comparing these two populations. Regardless of whether it is X-ray or radio selected, GC MSPs generally rotate slower than those in GF. For the X-ray emitting MSPs, since their \dot{E} are comparable in GCs and GF, the slower rotating GC MSPs suggests their surface magnetic field B_s should be stronger. Such expected difference can be seen by comparing their eCDFs and medians. With the outliers excluded in both GCs (i.e. M28 A) and GF (i.e. PSR J2018+4232 and PSR B1937+21), a difference between the X-ray selected MSPs in GCs and GF is suggested by both A-D and K-S tests ($p \sim 0.02$). A more significant difference of B_s between the radio selected MSPs in GCs and GF are indicated by both tests ($p \lesssim 5 \times 10^{-3}$). The conclusions are unaltered when the outliers are included in the comparison (Table 8 & Table 9).

6. SUMMARY AND DISCUSSION

We have performed a systematic analysis of the rotational, orbital and X-ray properties of MSPs in GCs and compared with those in the GF. The major results are summarized as follows:

1. GC MSPs generally rotate slower than those in the GF.
2. While X-ray observations tend to pick the MSPs with faster rotation in the GF, we do not find such selection effect in the GC MSP population.
3. Surface magnetic field (B_s) of GC MSPs are apparently stronger than those in the GF.
4. For the MSP binaries, strong correlation is found between the rotation period and the orbital period in the GF population. However, such correlation is absent in the GC MSP binaries.
5. Although the distributions of X-ray luminosity (L_x) and hardness (Γ) for the MSPs in GCs are comparable with those in the GF, the GC MSPs apparently follow a different $L_x - \dot{E}$ relation.

All these findings suggest that dynamical interactions in GCs can alter the evolution of MSPs/their progenitors and leave an imprint on their X-ray emission properties. Here we discuss the implications of our results.

One most distinguishable properties between the radio selected MSPs in GCs and GF is their distributions of P_b (Figure 10). It is clear that there is a lack of wide

orbit MSP binaries in GCs. This can be accounted by the frequent stellar encounters in GCs. Numerical studies have shown that close encounters between stars and binaries can affect the orbital parameters and dramatically alter the evolution of the binaries (Benacquista & Downing 2013). If the initial binding energy of a primordial binary is larger than the average kinetic energy of the neighboring stars in the cluster, the encounter can lead to orbital shrinkage with the orbital binding energy transferred to the neighboring stars (Heggie 1975).

It is instructive to compare the average orbital binding energy $\langle E_b \rangle$ of the radio selected GC MSPs with the averaged kinetic energy of the neighboring stars $\langle E_* \rangle$ in their hosting clusters. For each MSP binary, we computed E_b by $GM_{\text{psr}}M_c/2a$ where M_{psr} , M_c and a are the mass of pulsar, the mass of companion and the semi-major axis of the orbit respectively. We fixed M_{psr} at $1.35M_\odot$ for all systems. Both a and M_c are taken from the ATNF pulsar catalog (Manchester et al. 2005) by assuming an orbital inclination of $i = 60^\circ$. With these estimates, the average orbital energy of the radio selected GC MSP binaries is found to be $\langle E_b \rangle \sim 2.3 \times 10^{45}$ ergs. On the other hand, the corresponding value of the radio selected GF MSP binaries is $\langle E_b \rangle \sim 8.5 \times 10^{44}$ ergs which is about three times lower.

For $\langle E_* \rangle$, we calculated by averaging the characteristic value for each MSP-hosting GC. We computed E_* by $\frac{1}{2}M_*\sigma_*^2$, where M_* and σ_* are typical mass and the velocity dispersion of the neighboring stars in a GC. Values of σ_* were adopted from Harris (2010). For estimating M_* , we took the mass of a main sequence corresponding to the spectral type of the integrated cluster light for each GC given in Harris (2010). It is interesting to note that $\langle E_* \rangle \sim 1.6 \times 10^{45}$ ergs is rather close to the estimate of $\langle E_b \rangle$ for the GC MSP binaries. The similarity of these two quantities might indicate the past interactions between MSP binaries (and/or their progenitors) and the neighboring stars in the cluster, which can lead to equipartition among orbital energy, recoil kinetic energy of the binaries and the kinetic energy of the stars in GCs.

On the other hand, for any primordial binaries with wide orbits which have initial binding energy smaller than the average kinetic energy of the neighboring stars in the cluster, they are prone to be destroyed through the single-binary interaction (Heggie 1975; Benacquista & Downing 2013). All these can make the recycling process more complicated than their counterparts in the GF. This might explain the absence of $P_b - P$ correlation for the MSP binaries in GCs.

Disturbance on the recycling process for the MSPs in GCs might also account for their slower rotations.

Since mass transfer can be disrupted by the agitation of frequent stellar encounter (Verbunt & Freire 2014), this can leave the MSP with intermediate rotation period P which is consistent with our results.

We notice that Konar (2010) have reported an opposite conclusion (i.e. GC MSPs rotate *faster* than their counterparts in GF). The difference between their results and ours can be accounted by the difference in the adopted samples. While we selected the MSPs with the criterion $P < 20$ ms, Konar (2010) selected their sample with $P < 30$ ms. And most importantly, the sample size in our study is ~ 3 times larger than that adopted by Konar (2010). And we have more fast rotating MSPs in our sample. The average P of MSP in the GF/GCs are 7.75/5.70 ms in their sample (cf. Tab. 1 in Konar 2010). The corresponding values in our radio selected sample are found to be 3.73/4.34 ms (Table 9). On the other hand, with a much larger sample, our results confirm the scenario suggested by Verbunt & Freire (2014).

We have also examined whether such difference can be a result of observational effect. Since GC MSPs are generally located further than their GF counterparts, detecting fast rotating pulsars in GCs by radio observations can be more difficult because of the possible broadening of their pulses by scattering. This can possibly result in a MSP population in GCs with slower rotation than that in the GF. This prompts us to compare the pulse width between these two populations by taking the estimates of the pulse widths at 50% of their peaks in ATNF catalog (Manchester et al. 2005). Both A-D and K-S tests yield a p -value > 0.1 and hence there is no indication that the radio pulses of GC MSPs are broader.

Another evidence against the aforementioned hypothesis is the detection of the fastest known pulsars in Terzan 5, namely Terzan5 ad ($P \sim 1.4$ ms). Despite the fact that the pulsars in Terzan 5 have the highest dispersion measure among all MSPs, the discovery of Terzan5 ad shows that the improvement in instrumentation and search techniques in the radio surveys have greatly overcome the bias in detecting fast pulsars in GCs. For example, an effective temporal resolution of ~ 0.3 ms was achieved in the pulsar search towards Terzan 5 (Ransom et al. 2005; Hessels et al. 2006). Together with the fact that no known bias against the detection of slow pulsars, we do not find any convincing argument that the difference between the rotational period distributions of these two populations is a result of observational bias. Hence, we conclude the result that GC MSPs generally rotate slower than GF MSPs is intrinsic.

We also notice that the fraction of isolated MSPs in GCs is larger than that in the GF, which is particularly obvious in the X-ray selected sample (Figure 1). Verbunt & Freire (2014) have suggested that the large fraction of isolated MSPs in GCs can be a result of dynamical disruption. Although this is physically plausible, we would like to point out that this might also be an observational effect. In the GF, the X-ray counterparts of MSPs are detected by pointed observations towards individually chosen targets. This can lead to a selection bias towards those bright sources with interesting behavior such as spider pulsars. This can possibly account for their large fraction in the GF population and hence suppress the proportion of isolated MSPs. On the other hand, there is no such bias in searching X-ray counterparts of MSPs in GCs since all MSPs in a given GC are observed at once in the X-ray image. In view of this, we cannot exclude the possibility that the larger fraction of isolated MSPs in GCs is a result of observational bias. For resolving this issue, a systematic all-sky X-ray imaging survey on the GF will be needed (e.g. with eROSITA). With a less biased sample, the proportions of different classes of X-ray emitting MSPs can be re-examined.

For the radio selected samples, the larger fraction of isolated MSPs in GCs can also be a result of observational bias. Detecting MSPs in binaries is more challenging than detecting isolated MSPs because searches of orbital parameters are also required. For GCs, the situation is exacerbated by the intracluster acceleration. Any deviation of the timing solutions from the actual values might lead to smearing of the radio pulses which can hamper the detection. As a result, this can possibly lead to a larger proportion of isolated MSPs in GCs. Therefore, the conclusion of whether the dynamical disruption in GCs can lead to more isolated MSP is not without ambiguity.

During recycling, accretion on the neutron stars can induce the decay of the surface magnetic field through the processes such as Hall effect and Ohmic dissipation (Cumming et al. 2004). Therefore, perturbation on the spin-up process by the dynamical interactions can halt the magnetic field decay in GC MSPs. This is consistent with our findings that B_s of GC MSPs are larger than those in the GF (See Table 8 & 9). This inference has also been reported by Verbunt & Freire (2014) and Konar (2010). However, the ways how these studies collected their samples are different from our approach. It is unclear whether the estimates of \dot{P} adopted in these previous works have the acceleration terms corrected. It appears that these studies have collected those have larger \dot{P}_{obs} so as to have a smaller fractional contami-

nation attributed by the cluster acceleration. However, this unavoidably introduced the bias that favors the conclusion that B_s of GC MSPs is higher.

In our study, a majority of our samples of B_s are estimated by the \dot{P} with their acceleration terms corrected by long-term pulsar timing (see Table 4 and Section 4). Such correction is unlikely suffered from the aforementioned bias. However, as the measurement of time derivative of the orbital period \dot{P}_b should be easier for large P_b , most of the systems with intrinsic \dot{P} estimated by this method are non-spider MSP binaries. This can introduce another bias in this comparison as we do not know the B_s for the spider and isolated MSPs. On the other hand, Lee et al. (2018) found that all different types of MSPs in the GF have similar B_s (see Figure 6 in Lee et al. 2018). If this were also the case in GCs, our inference might remain be valid.

To understand the cause of the selection effect imposed by X-ray observations, we need to discuss the spin-down power \dot{E} of MSPs. In the GF, X-ray observations apparently pick the more powerful MSPs (i.e. larger \dot{E}) which are more luminous in X-ray as $L_x \propto \dot{E}^{1.31}$ (Lee et al. 2018). Since the distributions of B_s of both radio/X-ray selected samples in GF are similar and \dot{E} is proportional to B_s^2/P^4 , this explains why the X-ray emitting MSPs in GF generally rotate faster. Furthermore, because of the correlation between P and P_b , this also naturally explains why the X-ray emitting MSP binaries have tighter orbits in the GF.

However, in contrast to the situation in the GF, we do not find any evidence for the X-ray selection effect on the GC MSPs (see Table 8 & 9). We speculate that this might be accounted by the fact that the GC MSPs follow a different $L_x - \dot{E}$ relation. In our adopted sample, we found $L_x \propto \dot{E}^{0.4-0.8}$ (Table 10). It appears that the L_x of the GC MSPs have a less sensitive dependence on \dot{E} than those in the GF. This might explain why the selection effect on the GC population is less prominent than that in the GF.

For the GC MSPs, it is interesting to notice that the inferred dependence of their L_x on \dot{E} is consistent with that of Goldreich-Julian current $J_{GJ} \propto \sqrt{\dot{E}}$ (Goldreich & Julian 1969). This suggests that the X-rays are likely resulted from the polar cap heating by the back-flow current, which should be scaled with J_{GJ} . Since there is an indication that B_s is stronger in GC MSPs, this might facilitate the magnetic pair creation close to the stellar surface and result in a higher efficiency of polar cap heating than their GF counterparts (Cheng & Taam 2003). Also, Takata et al. (2010) suggest that if these magnetic pairs stream back to the outermagnetosphere, they will restrict the size of the outergap accelerator.

And hence the production of non-thermal emission will be limited. This is consistent with the fact that the X-rays from almost all the GC MSPs adopted in examining the $L_x - \dot{E}$ relation are thermal dominant (Table 2).

Lastly, we would like to highlight that the $L_x - \dot{E}$ relation for the GC MSPs reported in this work can be biased by the way we collected the sample. Since most of sample in Table 4 have the acceleration terms in their observed \dot{P} corrected by \dot{P}_b , it is biased by those having large P_b which are mostly non-spider MSP binaries. While we found that \dot{E} of the X-ray selected MSPs are comparable in GCs and GF, we are not sure how does this conclusion will be altered if the isolated and spider MSPs in GCs are included. In the GF, Lee et al. (2018) have shown that the \dot{E} of isolated and spider MSPs are comparable with each other and they are much larger than the non-spider MSPs (see Figure 7 and Table 4 in Lee et al. 2018). If the situation is similar in GC population, this might suggest that GC MSPs are more powerful than those in the GF. While measuring the line-of-sight acceleration of isolated and spider MSPs by long-term radio timing can be challenging, a systematic analysis of the whole GC MSP population with the mean-field acceleration and numerical simulation are encouraged for further investigation.

Recently, a new sub-class of BWs in the GF which are referred as *Tidarren* systems has been identified (Romani et al. 2016). While classic BWs have companion mass in a range of $\sim 0.02 - 0.05M_\odot$, the companions of Tidarren systems have mass $< 0.015M_\odot$ and with their hydrogen completely stripped off by the powerful pulsar wind. It has been suggested that they are descendants of the ultracompact X-ray binaries and follow a different evolutionary path. In a recent kinematic analysis of two Tidarren systems in the GF, Long et al. (2022) have shown that such systems can be originated from GCs. With more Tidarren systems discovered in the future, one can further examine the possible intricate relation between the MSPs in GCs and the GF.

During the reviewing process, we became aware that a publication by Zhao & Heinke (2022) on a similar subject as our work. The authors have also presented a population analysis of X-ray properties of GC MSPs but with a focus different from our work. While we have performed a systematic comparison between the MSPs in GCs and GF to explore the influence of dynamical interactions and the selection effects imposed by X-ray observations, Zhao & Heinke (2022) have focused solely on the X-ray properties of GC MSPs (e.g. examining their X-ray luminosity functions, placing upper and lower bounds on the number of MSPs in various GCs). On the other hand, their independent work allows

us to cross-check L_x and we found that the estimates in both works are consistent.

ACKNOWLEDGMENTS

The authors would like to thank Jongsuk Hong for the valuable comments and suggestions. J.L. is supported by the National Research Foundation of Korea grant 2016R1A5A1013277, 2022R1F1A1073952 and National Research Foundation of Korea grant funded by the Korean Government (NRF-2019H1A2A1077350-Global Ph.D. Fellowship Program); C.Y.H. is supported by the research fund of Chungnam National University and by the National Research Foundation of Korea grant 2022R1F1A1073952. J.T. are supported by the National Key Research and Development Program of China (grant No. 2020YFC2201400) and the National Natural Science Foundation of China (NSFC, grant No. 12173014). A.K.H.K. is supported by the National Science and Technology Council of Taiwan through grant 111-2112-M-007-020. P.H.T. is supported by the NSFC grant No. 12273122 and the China Manned Space Project (No. CMS-CSST-2021-B09). K.L.L. is supported by the National Science and Technology Council of the Republic of China (Taiwan) through grant 111-2636-M-006-024, and he is also a Yushan Young Fellow supported by the Ministry of Education of the Republic of China (Taiwan).

REFERENCES

- Ahnen, M. L., Ansoldi, S., Antonelli, L. A., et al. 2016, *A&A*, 593, A91, doi: [10.1051/0004-6361/201628447](https://doi.org/10.1051/0004-6361/201628447)
- Alpar, M. A., Cheng, A. F., Ruderman, M. A., & Shaham, J. 1982, *Nature*, 300, 728, doi: [10.1038/300728a0](https://doi.org/10.1038/300728a0)
- Amato, R., D’Ai, A., Del Santo, M., et al. 2019, *MNRAS*, 486, 3992, doi: [10.1093/mnras/stz1100](https://doi.org/10.1093/mnras/stz1100)
- Backer, D. C., Kulkarni, S. R., Heiles, C., Davis, M. M., & Goss, W. M. 1982, *Nature*, 300, 615, doi: [10.1038/300615a0](https://doi.org/10.1038/300615a0)
- Bahramian, A., Strader, J., Miller-Jones, J. C. A., et al. 2020, *ApJ*, 901, 57, doi: [10.3847/1538-4357/aba51d](https://doi.org/10.3847/1538-4357/aba51d)
- Bassa, C., Pooley, D., Homer, L., et al. 2004, *ApJ*, 609, 755, doi: [10.1086/421259](https://doi.org/10.1086/421259)
- Becker, W., Swartz, D. A., Pavlov, G. G., et al. 2003, *ApJ*, 594, 798, doi: [10.1086/376967](https://doi.org/10.1086/376967)
- Benacquista, M. J., & Downing, J. M. B. 2013, *Living Reviews in Relativity*, 16, 4, doi: [10.12942/lrr-2013-4](https://doi.org/10.12942/lrr-2013-4)
- Bhattacharya, S., Heinke, C. O., Chugunov, A. I., et al. 2017, *MNRAS*, 472, 3706, doi: [10.1093/mnras/stx2241](https://doi.org/10.1093/mnras/stx2241)
- Bogdanov, S., Bahramian, A., Heinke, C. O., et al. 2021, *ApJ*, 912, 124, doi: [10.3847/1538-4357/abee78](https://doi.org/10.3847/1538-4357/abee78)
- Bogdanov, S., & Grindlay, J. E. 2008, in *American Institute of Physics Conference Series*, Vol. 983, 40 Years of Pulsars: Millisecond Pulsars, Magnetars and More, ed. C. Bassa, Z. Wang, A. Cumming, & V. M. Kaspi, 64–68, doi: [10.1063/1.2900321](https://doi.org/10.1063/1.2900321)
- Bogdanov, S., Grindlay, J. E., Heinke, C. O., et al. 2006, *ApJ*, 646, 1104, doi: [10.1086/505133](https://doi.org/10.1086/505133)
- Bogdanov, S., van den Berg, M., Heinke, C. O., et al. 2010, *ApJ*, 709, 241, doi: [10.1088/0004-637X/709/1/241](https://doi.org/10.1088/0004-637X/709/1/241)
- Bogdanov, S., van den Berg, M., Servillat, M., et al. 2011, *ApJ*, 730, 81, doi: [10.1088/0004-637X/730/2/81](https://doi.org/10.1088/0004-637X/730/2/81)
- Cadelano, M., Ferraro, F. R., Istrate, A. G., et al. 2019, *ApJ*, 875, 25, doi: [10.3847/1538-4357/ab0e6b](https://doi.org/10.3847/1538-4357/ab0e6b)
- Cash, W. 1979, *ApJ*, 228, 939, doi: [10.1086/156922](https://doi.org/10.1086/156922)
- Cheng, K. S., & Taam, R. E. 2003, *ApJ*, 598, 1207, doi: [10.1086/379009](https://doi.org/10.1086/379009)
- Clark, G. W. 1975, *ApJL*, 199, L143, doi: [10.1086/181869](https://doi.org/10.1086/181869)

- Cognard, I., & Backer, D. C. 2004, *ApJL*, 612, L125, doi: [10.1086/424692](https://doi.org/10.1086/424692)
- Cognard, I., Bourgois, G., Lestrade, J. F., et al. 1996, *A&A*, 311, 179
- Cohn, H. N., Lugger, P. M., Zhao, Y., et al. 2021, *MNRAS*, 508, 2823, doi: [10.1093/mnras/stab2636](https://doi.org/10.1093/mnras/stab2636)
- Cumming, A., Arras, P., & Zweibel, E. 2004, *ApJ*, 609, 999, doi: [10.1086/421324](https://doi.org/10.1086/421324)
- Dai, S., Johnston, S., Kerr, M., et al. 2020, *ApJL*, 888, L18, doi: [10.3847/2041-8213/ab621a](https://doi.org/10.3847/2041-8213/ab621a)
- DeCesar, M. E., Ransom, S. M., Kaplan, D. L., Ray, P. S., & Geller, A. M. 2015, *ApJL*, 807, L23, doi: [10.1088/2041-8205/807/2/L23](https://doi.org/10.1088/2041-8205/807/2/L23)
- Du, Y., Qiao, G., Shuai, P., et al. 2015, *ApJ*, 801, 131, doi: [10.1088/0004-637X/801/2/131](https://doi.org/10.1088/0004-637X/801/2/131)
- Elsner, R. F., Heinke, C. O., Cohn, H. N., et al. 2008, *ApJ*, 687, 1019, doi: [10.1086/591899](https://doi.org/10.1086/591899)
- Fabian, A. C., Pringle, J. E., Verbunt, F., & Wade, R. A. 1983, *Nature*, 301, 222, doi: [10.1038/301222a0](https://doi.org/10.1038/301222a0)
- Forestell, L. M., Heinke, C. O., Cohn, H. N., et al. 2014, *MNRAS*, 441, 757, doi: [10.1093/mnras/stu559](https://doi.org/10.1093/mnras/stu559)
- Foster, R. S., Backer, D. C., Taylor, J. H., & Goss, W. M. 1988, *ApJL*, 326, L13, doi: [10.1086/185113](https://doi.org/10.1086/185113)
- Freire, P. C. C., Hessels, J. W. T., Nice, D. J., et al. 2005, *ApJ*, 621, 959, doi: [10.1086/427748](https://doi.org/10.1086/427748)
- Freire, P. C. C., Ransom, S. M., Bégin, S., et al. 2008a, *ApJ*, 675, 670, doi: [10.1086/526338](https://doi.org/10.1086/526338)
- Freire, P. C. C., & Ridolfi, A. 2018, *MNRAS*, 476, 4794, doi: [10.1093/mnras/sty524](https://doi.org/10.1093/mnras/sty524)
- Freire, P. C. C., Wolszczan, A., van den Berg, M., & Hessels, J. W. T. 2008b, *ApJ*, 679, 1433, doi: [10.1086/587832](https://doi.org/10.1086/587832)
- Freire, P. C. C., Ridolfi, A., Kramer, M., et al. 2017, *MNRAS*, 471, 857, doi: [10.1093/mnras/stx1533](https://doi.org/10.1093/mnras/stx1533)
- Goldreich, P., & Julian, W. H. 1969, *ApJ*, 157, 869, doi: [10.1086/150119](https://doi.org/10.1086/150119)
- Gregory, P. C., & Loredó, T. J. 1992, *ApJ*, 398, 146, doi: [10.1086/171844](https://doi.org/10.1086/171844)
- Grindlay, J. E., Camilo, F., Heinke, C. O., et al. 2002, *ApJ*, 581, 470, doi: [10.1086/344150](https://doi.org/10.1086/344150)
- Güver, T., & Özel, F. 2009, *MNRAS*, 400, 2050, doi: [10.1111/j.1365-2966.2009.15598.x](https://doi.org/10.1111/j.1365-2966.2009.15598.x)
- Harris, W. E. 1996, *AJ*, 112, 1487, doi: [10.1086/118116](https://doi.org/10.1086/118116)
- . 2010, arXiv e-prints, arXiv:1012.3224. <https://arxiv.org/abs/1012.3224>
- Heggie, D. C. 1975, *MNRAS*, 173, 729, doi: [10.1093/mnras/173.3.729](https://doi.org/10.1093/mnras/173.3.729)
- Heinke, C. O., Grindlay, J. E., Edmonds, P. D., et al. 2005, *ApJ*, 625, 796, doi: [10.1086/429899](https://doi.org/10.1086/429899)
- Henleywillis, S., Cool, A. M., Haggard, D., et al. 2018, *MNRAS*, 479, 2834, doi: [10.1093/mnras/sty675](https://doi.org/10.1093/mnras/sty675)
- Hermesen, W., Hessels, J. W. T., Kuiper, L., et al. 2013, *Science*, 339, 436, doi: [10.1126/science.1230960](https://doi.org/10.1126/science.1230960)
- Hessels, J. W. T., Ransom, S. M., Stairs, I. H., et al. 2006, *Science*, 311, 1901, doi: [10.1126/science.1123430](https://doi.org/10.1126/science.1123430)
- Huang, R. H. H., Kong, A. K. H., Takata, J., et al. 2012, *ApJ*, 760, 92, doi: [10.1088/0004-637X/760/1/92](https://doi.org/10.1088/0004-637X/760/1/92)
- Hui, C.-Y. 2018, *Journal of Korean Astronomical Society*, 51, 171, doi: [10.5303/JKAS.2018.51.6.171](https://doi.org/10.5303/JKAS.2018.51.6.171)
- Hui, C. Y., Cheng, K. S., & Taam, R. E. 2010, *ApJ*, 714, 1149, doi: [10.1088/0004-637X/714/2/1149](https://doi.org/10.1088/0004-637X/714/2/1149)
- Hui, C. Y., & Li, K. L. 2019, *Galaxies*, 7, 93, doi: [10.3390/galaxies7040093](https://doi.org/10.3390/galaxies7040093)
- Hui, C. Y., Tam, P. H. T., Takata, J., et al. 2014, *ApJL*, 781, L21, doi: [10.1088/2041-8205/781/1/L21](https://doi.org/10.1088/2041-8205/781/1/L21)
- Katz, J., Horwitz, G., & Klapisch, M. 1975, *ApJ*, 199, 307, doi: [10.1086/153693](https://doi.org/10.1086/153693)
- King, I. 1962, *AJ*, 67, 471, doi: [10.1086/108756](https://doi.org/10.1086/108756)
- Konar, S. 2010, *MNRAS*, 409, 259, doi: [10.1111/j.1365-2966.2010.17301.x](https://doi.org/10.1111/j.1365-2966.2010.17301.x)
- Lee, J., Hui, C. Y., Takata, J., et al. 2018, *ApJ*, 864, 23, doi: [10.3847/1538-4357/aad284](https://doi.org/10.3847/1538-4357/aad284)
- Lin, L. C.-C., Wang, H.-H., Hui, C. Y., et al. 2021, *MNRAS*, 503, 4908, doi: [10.1093/mnras/stab783](https://doi.org/10.1093/mnras/stab783)
- Linares, M., Bahramian, A., Heinke, C., et al. 2014, *MNRAS*, 438, 251, doi: [10.1093/mnras/stt2167](https://doi.org/10.1093/mnras/stt2167)
- Liu, W.-M., & Chen, W.-C. 2011, *MNRAS*, 416, 2285, doi: [10.1111/j.1365-2966.2011.19202.x](https://doi.org/10.1111/j.1365-2966.2011.19202.x)
- Long, J. S., Kong, A. K. H., Wu, K., et al. 2022, *The Astrophysical Journal*, 934, 17, doi: [10.3847/1538-4357/ac7720](https://doi.org/10.3847/1538-4357/ac7720)
- Lynch, R. S., Freire, P. C. C., Ransom, S. M., & Jacoby, B. A. 2012, *ApJ*, 745, 109, doi: [10.1088/0004-637X/745/2/109](https://doi.org/10.1088/0004-637X/745/2/109)
- Lynch, R. S., Ransom, S. M., Freire, P. C. C., & Stairs, I. H. 2011, *ApJ*, 734, 89, doi: [10.1088/0004-637X/734/2/89](https://doi.org/10.1088/0004-637X/734/2/89)
- Manchester, R. N., Hobbs, G. B., Teoh, A., & Hobbs, M. 2005, *AJ*, 129, 1993, doi: [10.1086/428488](https://doi.org/10.1086/428488)
- McKee, J. W., Janssen, G. H., Stappers, B. W., et al. 2016, *MNRAS*, 461, 2809, doi: [10.1093/mnras/stw1442](https://doi.org/10.1093/mnras/stw1442)
- Oh, K., Hui, C. Y., Li, K. L., & Kong, A. K. H. 2020, *MNRAS*, 498, 292, doi: [10.1093/mnras/staa2462](https://doi.org/10.1093/mnras/staa2462)
- Pallanca, C., Ransom, S. M., Ferraro, F. R., et al. 2014, *ApJ*, 795, 29, doi: [10.1088/0004-637X/795/1/29](https://doi.org/10.1088/0004-637X/795/1/29)
- Pallanca, C., Dalessandro, E., Ferraro, F. R., et al. 2010, *ApJ*, 725, 1165, doi: [10.1088/0004-637X/725/1/1165](https://doi.org/10.1088/0004-637X/725/1/1165)
- Papitto, A., Ferrigno, C., Bozzo, E., et al. 2013a, *Nature*, 501, 517, doi: [10.1038/nature12470](https://doi.org/10.1038/nature12470)

- Papitto, A., Hessels, J. W. T., Burgay, M., et al. 2013b, *The Astronomer's Telegram*, 5069, 1
- Pavlov, G. G., Kargaltsev, O., Garmire, G. P., & Wolszczan, A. 2007, *ApJ*, 664, 1072, doi: [10.1086/518926](https://doi.org/10.1086/518926)
- Possenti, A., Cerutti, R., Colpi, M., & Mereghetti, S. 2002, *A&A*, 387, 993, doi: [10.1051/0004-6361:20020472](https://doi.org/10.1051/0004-6361:20020472)
- Prager, B. J., Ransom, S. M., Freire, P. C. C., et al. 2017, *ApJ*, 845, 148, doi: [10.3847/1538-4357/aa7ed7](https://doi.org/10.3847/1538-4357/aa7ed7)
- Radhakrishnan, V., & Srinivasan, G. 1982, *Current Science*, 51, 1096
- Ransom, S. M., Hessels, J. W. T., Stairs, I. H., et al. 2005, *Science*, 307, 892, doi: [10.1126/science.1108632](https://doi.org/10.1126/science.1108632)
- Ransom, S. M., Stairs, I. H., Backer, D. C., et al. 2004, *ApJ*, 604, 328, doi: [10.1086/381730](https://doi.org/10.1086/381730)
- Richer, H. B., Fahlman, G. G., Ibata, R. A., et al. 1997, *ApJ*, 484, 741, doi: [10.1086/304379](https://doi.org/10.1086/304379)
- Ridolfi, A., Freire, P. C. C., Gupta, Y., & Ransom, S. M. 2019, *MNRAS*, 490, 3860, doi: [10.1093/mnras/stz2645](https://doi.org/10.1093/mnras/stz2645)
- Ridolfi, A., Freire, P. C. C., Torne, P., et al. 2016, *MNRAS*, 462, 2918, doi: [10.1093/mnras/stw1850](https://doi.org/10.1093/mnras/stw1850)
- Ridolfi, A., Gautam, T., Freire, P. C. C., et al. 2021, *MNRAS*, 504, 1407, doi: [10.1093/mnras/stab790](https://doi.org/10.1093/mnras/stab790)
- Romani, R. W., Graham, M. L., Filippenko, A. V., & Zheng, W. 2016, *ApJ*, 833, 138, doi: [10.3847/1538-4357/833/2/138](https://doi.org/10.3847/1538-4357/833/2/138)
- Scargle, J. D., Norris, J. P., Jackson, B., & Chiang, J. 2013, *ApJ*, 764, 167, doi: [10.1088/0004-637X/764/2/167](https://doi.org/10.1088/0004-637X/764/2/167)
- Sereno, M. 2016, *MNRAS*, 455, 2149, doi: [10.1093/mnras/stv2374](https://doi.org/10.1093/mnras/stv2374)
- Stephens, M. A. 1970, *Journal of the Royal Statistical Society. Series B (Methodological)*, 32, 115. <http://www.jstor.org/stable/2984408>
- Strickler, R. R., Cool, A. M., Anderson, J., et al. 2009, *ApJ*, 699, 40, doi: [10.1088/0004-637X/699/1/40](https://doi.org/10.1088/0004-637X/699/1/40)
- Takata, J., Wang, Y., & Cheng, K. S. 2010, *ApJ*, 715, 1318, doi: [10.1088/0004-637X/715/2/1318](https://doi.org/10.1088/0004-637X/715/2/1318)
- Takata, J., Li, K. L., Leung, G. C. K., et al. 2014, *ApJ*, 785, 131, doi: [10.1088/0004-637X/785/2/131](https://doi.org/10.1088/0004-637X/785/2/131)
- Takata, J., Wang, H. H., Lin, L. C. C., et al. 2020, *ApJ*, 890, 16, doi: [10.3847/1538-4357/ab67b1](https://doi.org/10.3847/1538-4357/ab67b1)
- Tauris, T. M. 2011, in *Astronomical Society of the Pacific Conference Series*, Vol. 447, *Evolution of Compact Binaries*, ed. L. Schmidtbreick, M. R. Schreiber, & C. Tappert, 285. <https://arxiv.org/abs/1106.0897>
- Tauris, T. M., & Savonije, G. J. 1999, *A&A*, 350, 928. <https://arxiv.org/abs/astro-ph/9909147>
- Toscano, M., Sandhu, J. S., Bailes, M., et al. 1999, *MNRAS*, 307, 925, doi: [10.1046/j.1365-8711.1999.02685.x](https://doi.org/10.1046/j.1365-8711.1999.02685.x)
- Turk, P. J., & Lorimer, D. R. 2013, *MNRAS*, 436, 3720, doi: [10.1093/mnras/stt1850](https://doi.org/10.1093/mnras/stt1850)
- Valenti, E., Ferraro, F. R., & Origlia, L. 2007, *AJ*, 133, 1287, doi: [10.1086/511271](https://doi.org/10.1086/511271)
- Verbunt, F., & Freire, P. C. C. 2014, *A&A*, 561, A11, doi: [10.1051/0004-6361/201321177](https://doi.org/10.1051/0004-6361/201321177)
- Vleschow, L., Stappers, B. W., Bailes, M., et al. 2022, *MNRAS*, 513, 1386, doi: [10.1093/mnras/stac921](https://doi.org/10.1093/mnras/stac921)
- Wang, L., Peng, B., Stappers, B. W., et al. 2020, *ApJ*, 892, 43, doi: [10.3847/1538-4357/ab76cc](https://doi.org/10.3847/1538-4357/ab76cc)
- Willis, J. P., Oguri, M., Ramos-Ceja, M. E., et al. 2021, *MNRAS*, 503, 5624, doi: [10.1093/mnras/stab873](https://doi.org/10.1093/mnras/stab873)
- Zavlin, V. E. 2007, *Ap&SS*, 308, 297, doi: [10.1007/s10509-007-9297-y](https://doi.org/10.1007/s10509-007-9297-y)
- Zhang, L., & Cheng, K. S. 2003, *A&A*, 398, 639, doi: [10.1051/0004-6361:20021570](https://doi.org/10.1051/0004-6361:20021570)
- Zhao, J., & Heinke, C. O. 2022, *MNRAS*, 511, 5964, doi: [10.1093/mnras/stac442](https://doi.org/10.1093/mnras/stac442)
- Zhao, J., Zhao, Y., & Heinke, C. O. 2021, *MNRAS*, 502, 1596, doi: [10.1093/mnras/stab117](https://doi.org/10.1093/mnras/stab117)

Table 1. List of *Chandra* ACIS observations of GCs with MSPs identified.

Obs.ID	Start Date and Time (UTC)	Inst. (ACIS-)	Exp. time (ks)	Obs.ID	Start Date and Time (UTC)	Inst. (ACIS-)	Exp. time (ks)
NGC1851				NGC104 (47Tuc)			
8966	2008-04-04T15:32:24	S	18.80	953	2000-03-16T08:38:40	I	31.67
15734	2015-02-04T21:01:44	S	19.80	955	2000-03-16T18:32:00	I	31.67
17588	2015-02-07T13:28:34	S	27.67	2735	2002-09-29T16:57:56	S	65.24
NGC5139 (ω Cen)				NGC6397			
653	2000-01-24T02:13:58	I	25.03	2736	2002-09-30T13:24:28	S	65.24
1519	2000-01-25T04:32:36	I	43.59	2737	2002-10-02T18:50:07	S	65.24
13727	2012-04-16T06:18:36	I	48.53	2738	2002-10-11T01:41:55	S	68.77
13726	2012-04-17T08:16:43	I	173.74	16527	2014-09-05T04:38:37	S	40.88
NGC5272 (M3)				Terzan5			
4543	2004-05-09T17:26:32	S	10.15	15747	2014-09-09T19:32:57	S	50.04
NGC5904 (M5)				NGC6626 (M28)			
2676	2002-09-24T06:51:22	S	44.66	2684	2002-07-04T18:02:19	S	12.75
NGC6121 (M4)				NGC6656 (M22)			
946	2000-06-30T04:24:23	S	25.82	5437	2005-05-24T21:21:23	S	15.82
7447	2007-07-06T05:26:35	S	45.46	14609	2014-05-22T19:39:17	S	84.86
7446	2007-09-18T02:47:24	S	47.93	NGC6760			
NGC6205 (M13)				NGC6752			
7290	2006-03-09T23:01:13	S	27.89	948	2000-05-15T04:36:02	S	29.47
5436	2006-03-11T06:19:34	S	26.80	6612	2006-02-10T22:48:48	S	37.97
NGC6266 (M62)				NGC6752			
2677	2002-05-12T09:12:42	S	62.27	19014	2017-07-02T03:27:25	S	98.81
15761	2014-05-05T19:18:39	S	82.09	19013	2017-07-24T09:33:12	S	43.20
NGC6440				NGC6752			
947	2000-07-04T13:28:39	S	23.28	20121	2017-07-25T17:04:15	S	18.26
3799	2003-06-27T08:57:31	S	24.05	20122	2017-07-29T09:00:43	S	67.22
10060	2009-07-28T15:05:44	S	49.11	20123	2017-07-30T23:53:18	S	49.46
NGC6441				NGC6752			
9598	2008-06-22T22:06:39	S	17.97	NGC6752			
9874	2008-06-24T08:51:51	S	16.96	NGC6752			
NGC6517				NGC6752			
9597	2009-02-04T14:22:23	S	23.62	NGC6752			
NGC6544				NGC6752			
5435	2005-07-20T14:59:58	S	16.28	NGC6752			
NGC6652				NGC6752			
12461	2011-06-03T21:35:28	S	45.32	NGC6752			
18987	2017-05-22T08:13:22	S	10.04	NGC6752			
NGC6656 (M22)				NGC6752			
5437	2005-05-24T21:21:23	S	15.82	NGC6752			
14609	2014-05-22T19:39:17	S	84.86	NGC6752			
NGC6760				NGC6752			
13672	2012-06-27T17:09:21	S	51.38	NGC6752			
NGC6838 (M71)				NGC6752			
5434	2004-12-20T15:18:45	S	52.45	NGC6752			
NGC7099 (M30)				NGC6752			
2679	2001-11-19T02:55:12	S	49.43	NGC6752			
20725	2017-09-04T16:33:05	S	17.49	NGC6752			
18997	2017-09-06T00:05:19	S	90.19	NGC6752			
20726	2017-09-10T02:09:13	S	19.21	NGC6752			
20732	2017-09-14T14:23:17	S	47.90	NGC6752			
20731	2017-09-16T18:04:17	S	23.99	NGC6752			
20792	2017-09-18T04:21:43	S	36.86	NGC6752			
20795	2017-09-22T11:39:56	S	14.33	NGC6752			
20796	2017-09-23T06:09:30	S	30.68	NGC6752			

Note. Only observations with the effective exposure > 10 ks are used in our analysis. Data with shorter exposure (e.g. those were acquired from TOO/DDT requests) are excluded because either they do not provide sufficient photon statistics or they are affected by nearby outbursts.

Table 2. Properties of 56 X-ray detected MSPs in GCs.

MSP Name	R.A. (J2000) (h : m : s)	Dec. (J2000) (° : ′ : ″)	P (ms)	Class ^a	P_b (day)	Thermal (T) / Non-thermal (NT)	Γ	$\log_{10} L_x^{0.3-8}$ (erg/s)	$\log_{10} L_x^{2-10}$ (erg/s)	Ref.
NGC104 (47Tuc) / $d = 4.5$ kpc (Harris 1996)										
47Tuc aa	00:24:07.31	-72:05:19.40	1.840	Iso	..	T	$2.13^{+0.39}_{-0.36}$	$30.35^{+0.10}_{-0.09}$	$29.98^{+0.24}_{-0.27}$	1,2,3*
47Tuc ab	00:24:08.10	-72:04:47.88	3.705	Iso	..	T	$2.43^{+0.17}_{-0.16}$	$30.81^{+0.03}_{-0.04}$	$30.28^{+0.11}_{-0.11}$	2,3*,4
47Tuc C	00:23:50.36	-72:04:31.51	5.767	Iso	..	T	$2.89^{+0.41}_{-0.39}$	$30.35^{+0.08}_{-0.08}$	$29.52^{+0.26}_{-0.28}$	2,4,5*
47Tuc D	00:24:13.88	-72:04:43.85	5.358	Iso	..	T	$2.44^{+0.21}_{-0.20}$	$30.74^{+0.04}_{-0.04}$	$30.20^{+0.14}_{-0.14}$	2,4,5*
47Tuc E	00:24:11.11	-72:05:20.15	3.536	Oth	2.257	T	$3.01^{+0.20}_{-0.19}$	$30.88^{+0.04}_{-0.04}$	$29.97^{+0.13}_{-0.14}$	2,4,5*
47Tuc H	00:24:06.70	-72:04:06.81	3.210	Oth	2.358	T	$3.15^{+0.28}_{-0.27}$	$30.64^{+0.06}_{-0.06}$	$29.63^{+0.18}_{-0.18}$	2,4,5*
47Tuc J	00:23:59.41	-72:03:58.79	2.101	BW	0.127	NT	$2.05^{+0.16}_{-0.15}$	$30.92^{+0.04}_{-0.04}$	$30.58^{+0.10}_{-0.10}$	2,4,5*
47Tuc L	00:24:03.77	-72:04:56.92	4.346	Iso	..	T	$2.66^{+0.11}_{-0.11}$	$31.13^{+0.02}_{-0.02}$	$30.45^{+0.07}_{-0.07}$	2,4,5*
47Tuc M	00:23:54.49	-72:05:30.76	3.677	Iso	..	T	$2.55^{+0.31}_{-0.29}$	$30.53^{+0.07}_{-0.07}$	$29.92^{+0.19}_{-0.20}$	2,4,5*
47Tuc N	00:24:09.19	-72:04:28.89	3.054	Iso	..	T	$2.47^{+0.24}_{-0.24}$	$30.60^{+0.05}_{-0.05}$	$30.05^{+0.16}_{-0.16}$	2,4,5*
47Tuc O	00:24:04.65	-72:04:53.77	2.643	BW	0.136	NT	$2.62^{+0.12}_{-0.12}$	$31.01^{+0.03}_{-0.03}$	$30.35^{+0.08}_{-0.08}$	2,4,5*
47Tuc Q	00:24:16.49	-72:04:25.16	4.033	Oth	1.189	T	$2.63^{+0.26}_{-0.25}$	$30.62^{+0.05}_{-0.05}$	$29.96^{+0.16}_{-0.17}$	2,4,5*
47Tuc R	00:24:07.59	-72:04:50.40	3.480	BW	0.066	T	$2.61^{+0.15}_{-0.15}$	$30.93^{+0.03}_{-0.03}$	$30.28^{+0.10}_{-0.10}$	2,4,5*
47Tuc T	00:24:08.55	-72:04:38.93	7.588	Oth	1.126	T	$2.49^{+0.32}_{-0.31}$	$30.50^{+0.06}_{-0.06}$	$29.93^{+0.20}_{-0.21}$	2,4,5*
47Tuc U	00:24:09.84	-72:03:59.69	4.343	Oth	0.429	T	$2.41^{+0.24}_{-0.23}$	$30.73^{+0.05}_{-0.05}$	$30.21^{+0.14}_{-0.15}$	2,4,5*
47Tuc W	00:24:06.06	-72:04:49.03	2.352	RB	0.133	NT	$1.63^{+0.07}_{-0.07}$	$31.35^{+0.02}_{-0.02}$	$31.19^{+0.04}_{-0.04}$	2,5*,6
47Tuc X	00:24:22.42	-72:01:17.29	4.772	Oth	10.921	T	$2.94^{+0.44}_{-0.41}$	$30.51^{+0.09}_{-0.09}$	$29.65^{+0.25}_{-0.26}$	2,6*
47Tuc Y	00:24:01.40	-72:04:41.84	2.197	Oth	0.522	T	$3.04^{+0.25}_{-0.24}$	$30.65^{+0.05}_{-0.05}$	$29.72^{+0.15}_{-0.16}$	2,4,5*
47Tuc Z	00:24:06.02	-72:05:01.65	4.554	Iso	..	T	$2.63^{+0.17}_{-0.16}$	$30.86^{+0.03}_{-0.03}$	$30.20^{+0.11}_{-0.11}$	2,3*,4
NGC 5139 (ω Cen) / $d = 5.2$ kpc (Harris 1996)										
ω Cen A	13:26:39.67	-47:30:11.64	4.109	Iso	$2.87^{+1.47}_{-1.32}$	$30.31^{+0.45}_{-0.25}$	$29.50^{+0.64}_{-0.72}$	2,7,8*
ω Cen B	13:26:49.57	-47:29:24.18	4.792	BW	0.090	..	$1.94^{+0.69}_{-0.63}$	$30.75^{+0.14}_{-0.15}$	$30.47^{+0.33}_{-0.36}$	2,7,8*,9
NGC6121 (M4) / $d = 1.73$ kpc (Richer et al. 1997)										
M4 A	16:23:38.21	-26:31:54.21	11.076	Oth	191.443	..	$3.03^{+0.32}_{-0.30}$	$30.47^{+0.10}_{-0.09}$	$29.54^{+0.16}_{-0.16}$	2,10,11*
NGC6205 (M13) / $d = 7.1$ kpc (Harris 1996)										
M13 B	16:41:40.39	36:25:58.49	3.528	Oth	1.259	NT	$1.80^{+0.70}_{-0.30}$	$30.90^{+0.18}_{-0.30}$	$30.70^{+0.18}_{-0.30}$	12,13*
M13 C	16:41:41.01	36:27:02.74	3.722	Iso	..	T	$3.90^{+1.20}_{-0.48}$	$30.73^{+0.22}_{-0.48}$	$29.15^{+0.22}_{-0.48}$	12,13*
M13 D	16:41:42.40	36:27:28.20	3.118	Oth	0.591	T	$3.70^{+0.90}_{-0.34}$	$30.89^{+0.19}_{-0.14}$	$29.74^{+0.24}_{-0.30}$	12,13*
M13 E	16:41:42.02	36:27:34.97	2.487	BW	0.113	NT	$2.20^{+0.60}_{-0.20}$	$31.06^{+0.14}_{-0.15}$	$30.57^{+0.13}_{-0.15}$	12,13*
M13 F	16:41:44.61	36:28:16.00	3.004	Oth	1.378	T	$3.70^{+0.70}_{-0.22}$	$31.08^{+0.15}_{-0.22}$	$29.75^{+0.12}_{-0.13}$	12,13*
NGC6266 (M62) / $d = 6.8$ kpc (Harris 1996)										
M62 B	17:01:12.70	-30:06:48.87	3.594	RB	0.145	NT	$2.17^{+0.21}_{-0.20}$	$31.95^{+0.04}_{-0.04}$	$31.56^{+0.09}_{-0.10}$	14*
M62 C	17:01:12.92	-30:06:59.09	7.613	Oth	0.215	NT	$2.42^{+0.39}_{-0.08}$	$31.65^{+0.08}_{-0.06}$	$31.12^{+0.19}_{-0.19}$	14*
NGC6397 / $d = 2.4$ kpc (Strickler et al. 2009)										
NGC6397 A	17:40:44.57	-53:40:41.84	3.650	RB	1.354	NT	$1.85^{+0.07}_{-0.02}$	$31.35^{+0.01}_{-0.02}$	$31.11^{+0.03}_{-0.03}$	15*
Terzan5 / $d = 5.9$ kpc (Valenti et al. 2007)										
Terzan5 A	17:48:02.25	-24:46:37.91	11.563	RB	0.076	NT	$1.24^{+0.69}_{-0.16}$	$31.95^{+0.12}_{-0.16}$	$31.91^{+0.12}_{-0.16}$	16*
Terzan5 E	17:48:03.41	-24:46:35.78	2.198	Oth	60.060	..	2.00^b	$30.49^{+0.14}_{-0.14}$	$30.18^{+0.14}_{-0.14}$	16*
Terzan5 F	17:48:05.11	-24:46:38.16	5.554	Iso	2.00^b	$30.95^{+0.12}_{-0.12}$	$30.64^{+0.12}_{-0.12}$	16*
Terzan5 H	17:48:05.62	-24:46:53.24	4.926	Iso	2.00^b	$30.86^{+0.14}_{-0.14}$	$30.55^{+0.14}_{-0.14}$	16*
Terzan5 K	17:48:03.90	-24:46:47.84	2.970	Iso	2.00^b	$30.35^{+0.15}_{-0.15}$	$30.04^{+0.15}_{-0.15}$	16*
Terzan5 L	17:48:04.74	-24:46:35.75	2.245	Iso	2.00^b	$31.15^{+0.09}_{-0.09}$	$30.84^{+0.09}_{-0.09}$	16*
Terzan5 N	17:48:04.91	-24:46:54.00	8.667	Oth	0.386	..	2.00^b	$30.40^{+0.13}_{-0.13}$	$30.09^{+0.13}_{-0.13}$	16*
Terzan5 O	17:48:04.69	-24:46:51.41	1.677	BW	0.260	..	2.00^b	$31.46^{+0.04}_{-0.04}$	$31.15^{+0.04}_{-0.04}$	16*
Terzan5 P	17:48:05.04	-24:46:41.40	1.396	RB	0.363	NT	$0.86^{+0.17}_{-0.16}$	$32.59^{+0.03}_{-0.03}$	$32.28^{+0.03}_{-0.03}$	16*
Terzan5 Q	17:48:04.33	-24:47:05.12	2.812	Oth	30.295	..	2.00^b	$30.11^{+0.19}_{-0.19}$	$29.81^{+0.17}_{-0.17}$	16*
Terzan5 V	17:48:05.09	-24:46:34.63	2.073	Oth	0.504	..	2.00^b	$31.29^{+0.06}_{-0.06}$	$30.98^{+0.06}_{-0.06}$	16*
Terzan5 X	17:48:05.59	-24:47:12.14	2.999	Oth	4.999	..	2.00^b	$30.71^{+0.15}_{-0.15}$	$30.40^{+0.15}_{-0.15}$	16*
Terzan5 Z	17:48:04.95	-24:46:46.04	2.463	Oth	3.488	..	2.00^b	$31.06^{+0.07}_{-0.07}$	$30.76^{+0.07}_{-0.07}$	16*
Terzan5 ad	17:48:03.85	-24:46:41.94	1.729	RB	1.094	NT	$1.16^{+0.24}_{-0.22}$	$32.30^{+0.04}_{-0.04}$	$32.89^{+0.04}_{-0.04}$	16*
NGC6626 (M28) / $d = 5.5$ kpc (Harris 1996)										
M28 A	18:24:32.01	-24:52:10.83	3.054	Iso	..	NT	$1.21^{+0.02}_{-0.02}$	$33.15^{+0.01}_{-0.01}$	$33.12^{+0.01}_{-0.12}$	2,17*
M28 G	18:24:33.03	-24:52:17.32	5.909	BW	0.105	NT	$2.89^{+0.25}_{-0.25}$	$31.29^{+0.07}_{-0.07}$	$30.47^{+0.12}_{-0.13}$	2,17*
M28 H	18:24:31.61	-24:52:17.20	4.629	RB	0.435	NT	$1.11^{+0.19}_{-0.19}$	$31.34^{+0.06}_{-0.05}$	$31.33^{+0.09}_{-0.09}$	2,17*,18
M28 I	18:24:32.53	-24:52:08.60	3.932	RB	0.459	NT	$1.46^{+0.28}_{-0.28}$	$32.46^{+0.68}_{-0.68}$	$32.36^{+0.68}_{-0.68}$	2,19*,20
M28 L	18:24:32.35	-24:52:08.02	4.100	BW	0.226	NT	$1.40^{+0.06}_{-0.06}$	$32.27^{+0.02}_{-0.02}$	$32.19^{+0.03}_{-0.03}$	2,17*,21
NGC6656 (M22) / $d = 3.2$ kpc (Harris 1996)										
M22 A	18:36:25.50	-23:54:51.50	3.350	BW	0.203	..	$1.50^{+0.70}_{-0.60}$	$30.47^{+0.12}_{-0.12}$	$30.38^{+0.12}_{-0.12}$	22*
NGC6752 / $d = 4.0$ kpc (Harris 1996)										
NGC6752 A	19:11:42.76	-59:58:26.90	3.266	Oth	0.837	T	$3.06^{+0.49}_{-0.47}$	$30.86^{+0.15}_{-0.14}$	$29.91^{+0.24}_{-0.26}$	2,23*
NGC6752 B	19:10:52.05	-59:59:00.75	8.358	Iso	..	T	$3.40^{+1.53}_{-1.45}$	$30.76^{+0.49}_{-0.27}$	$29.56^{+0.83}_{-0.78}$	2,23*
NGC6752 C	19:11:05.56	-60:00:59.70	5.277	Iso	..	T	$2.51^{+0.36}_{-0.34}$	$30.69^{+0.08}_{-0.08}$	$30.11^{+0.19}_{-0.20}$	2,23*
NGC6752 D	19:10:52.42	-59:59:05.50	9.034	Iso	..	T	$2.60^{+0.27}_{-0.27}$	$30.92^{+0.05}_{-0.05}$	$30.28^{+0.16}_{-0.16}$	2,23*
NGC6752 F	19:10:52.07	-59:59:09.41	4.143	Iso	$2.30^{+0.65}_{-0.65}$	$30.93^{+0.20}_{-0.20}$	$30.47^{+0.20}_{-0.20}$	2,24,25*
NGC6838 (M71) / $d = 4.0$ kpc (Harris 1996)										
M71 A	19:53:46.42	18:47:04.91	4.888	BW	0.177	NT	$1.85^{+0.33}_{-0.31}$	$31.19^{+0.07}_{-0.07}$	$30.95^{+0.16}_{-0.16}$	2,26*

Note.

^a Different classes of MSPs: Iso (Isolated MSP), RB (Redback), BW (Black-widow), and Oth (Others binary).

^b Following Bogdanov et al. (2021), a single power-law model with Γ fixed at 2 are adopted for these cases because of the small photon statistics.

Ref. (1) Freire & Ridolfi (2018) (2) this work (3) Bhattacharya et al. (2017) (4) Freire et al. (2017) (5) Bogdanov et al. (2006) (6) Ridolfi et al. (2016) (7) Dai et al. (2020) (8) Zhao & Heinke (2022) (9) Henleywillis et al. (2018) (10) Bassa et al. (2004) (11) Pavlov et al. (2007) (12) Wang et al. (2020) (13) Zhao et al. (2021) (14) Oh et al. (2020) (15) Bogdanov et al. (2010) (16) Bogdanov et al. (2021) (17) Bogdanov et al. (2011) (18) Pallanca et al. (2010) (19) Papitto et al. (2013a) (20) Linares et al. (2014) (21) Becker et al. (2003) (22) Amato et al. (2019) (23) Forestell et al. (2014) (24) Ridolfi et al. (2021) (25) Cohn et al. (2021) (26) Elsner et al. (2008) The entries marked with * are the references which have the identifications of the X-ray counterparts of GC MSPs reported.

Table 3. Upper limits of L_x of 60 GC MSPs.

MSP Name	R.A. (J2000) (h : m : s)	Dec. (J2000) ($^{\circ}$: $'$: $''$)	P (ms)	Class	P_b (day)	$\log_{10} L_x^{0.3-8}$ (erg/s)	$\log_{10} L_x^{2-10}$ (erg/s)	Ref.
NGC104 (47Tuc) / $d = 4.5$ kpc (Harris 1996)								
47Tuc F	00:24:03.86	-72:04:42.82	2.624	Iso	..	≤ 30.01	≤ 29.64	1
47Tuc G	00:24:07.96	-72:04:39.70	4.040	Iso	..	≤ 30.01	≤ 29.64	1
47Tuc I	00:24:07.93	-72:04:39.68	3.485	BW	0.230	≤ 30.01	≤ 29.64	1
47Tuc P	00:24:2s0	-72:04:10	3.643	BW	0.147	≤ 30.01	≤ 29.64	2
47Tuc S	00:24:03.98	-72:04:42.35	2.830	Oth	1.201	≤ 30.01	≤ 29.64	1
47Tuc V	00:24:05.36	-72:04:53.20	4.810	Oth	0.227	≤ 30.01	≤ 29.64	2
NGC1851 / $d = 12.1$ kpc (Harris 1996)								
NGC1851 A	05:14:06.69	-40:02:48.89	4.991	Oth	18.785	≤ 31.96	≤ 31.65	3
NGC5272 (M3) / $d = 10.2$ kpc (Harris 1996)								
M3 B	13:42:11.09	28:22:40.14	2.389	Oth	1.417	≤ 32.82	≤ 31.81	4
M3 D	13:42:10.20	28:22:36.00	5.443	Oth	128.752	≤ 32.82	≤ 31.81	4
NGC5904 (M5) / $d = 7.5$ kpc (Harris 1996)								
M5 A	15:18:33.32	02:05:27.44	5.554	Iso	..	≤ 31.41	≤ 31.04	5
M5 B	15:18:31.46	02:05:15.30	7.947	Oth	6.859	≤ 31.41	≤ 31.04	5
M5 C	15:18:32.79	02:04:47.82	2.484	BW	0.087	≤ 31.41	≤ 31.04	6
NGC6205 (M13) / $d = 7.1$ kpc (Harris 1996)								
M13 A	16:41:40.87	36:27:14.98	10.38	Iso	..	≤ 31.43	≤ 31.12	7
NGC6266 (M62) / $d = 6.9$ kpc (Harris 1996)								
M62 A	17:01:12.51	-30:06:30.17	5.242	Oth	3.806	≤ 31.04	≤ 30.73	8
M62 D	17:01:13.56	-30:06:42.56	3.418	Oth	1.118	≤ 31.04	≤ 30.73	8
M62 E	17:01:13.27	-30:06:46.89	3.234	BW	0.159	≤ 31.04	≤ 30.73	8
M62 F	17:01:12.82	-30:06:51.82	2.295	BW	0.206	≤ 31.04	≤ 30.73	8
M62 G	17:01:14.00	-30:06:42.00	4.608	Oth	0.774	≤ 31.04	≤ 30.73	9
NGC6440 / $d = 8.5$ kpc (Harris 1996)								
NGC6440 B	17:48:52.76	-20:21:38.45	16.760	Oth	20.550	≤ 31.72	≤ 31.41	10
NGC6440 C	17:48:51.17	-20:21:53.81	6.227	Iso	..	≤ 31.72	≤ 31.41	11
NGC6440 D	17:48:51.65	-20:21:07.41	13.496	RB	0.286	≤ 31.72	≤ 31.41	11
NGC6440 E	17:48:52.80	-20:21:29.38	16.264	Iso	..	≤ 31.72	≤ 31.41	11
NGC6440 F	17:48:52.33	-20:21:39.33	3.794	Oth	9.834	≤ 31.72	≤ 31.41	11
Terzan5 / $d = 5.9$ kpc (Valenti et al. 2007)								
Terzan5 C	17:48:04.52	-24:46:35.17	8.436	Iso	..	≤ 31.80	≤ 31.49	12
Terzan5 D	17:48:05.93	-24:46:06.05	4.714	Iso	..	≤ 31.80	≤ 31.49	12
Terzan5 I	17:48:04.85	-24:46:46.37	9.570	Oth	1.300	≤ 31.80	≤ 31.49	12
Terzan5 M	17:48:04.62	-24:46:40.75	3.570	Oth	0.443	≤ 31.80	≤ 31.49	12
Terzan5 R	17:48:04.69	-24:46:50.25	5.029	Iso	..	≤ 31.80	≤ 31.49	12
Terzan5 S	17:48:04.29	-24:46:31.71	6.117	Iso	..	≤ 31.80	≤ 31.49	12
Terzan5 T	17:48:02.99	-24:46:52.81	7.045	Iso	..	≤ 31.80	≤ 31.49	12
Terzan5 U	17:48:04.24	-24:46:47.86	3.289	Oth	3.600	≤ 31.80	≤ 31.49	12
Terzan5 W	17:48:04.84	-24:46:42.38	4.205	Oth	4.877	≤ 31.80	≤ 31.49	12
Terzan5 Y	17:48:05.10	-24:46:44.57	2.048	Oth	1.170	≤ 31.80	≤ 31.49	12
Terzan5 aa	17:48:05.81	-24:46:42.24	5.788	Iso	..	≤ 31.80	≤ 31.49	12
Terzan5 ab	17:48:04.76	-24:46:42.65	5.120	Iso	..	≤ 31.80	≤ 31.49	12
Terzan5 ac	17:48:06.04	-24:46:32.53	5.087	Iso	..	≤ 31.80	≤ 31.49	12
Terzan5 ae	17:48:04.96	-24:46:45.72	3.659	BW	0.171	≤ 31.80	≤ 31.49	12
Terzan5 af	17:48:04.21	-24:46:45.72	3.304	Iso	..	≤ 31.80	≤ 31.49	12
Terzan5 ag	17:48:04.81	-24:46:34.59	4.448	Iso	..	≤ 31.80	≤ 31.49	12
Terzan5 ah	17:48:04.32	-24:46:42.03	4.965	Iso	..	≤ 31.80	≤ 31.49	12
Terzan5 aj	17:48:05.01	-24:46:34.69	2.959	Iso	..	≤ 31.80	≤ 31.49	12
Terzan5 ak	17:48:03.69	-24:46:37.93	1.890	Iso	..	≤ 31.80	≤ 31.49	12
NGC6441 / $d = 11.6$ kpc (Harris 1996)								
NGC6441 B	17:50:12.18	-37:03:22.93	6.075	Oth	3.605	≤ 32.18	≤ 31.80	11
NGC6441 D	17:50:13.10	-37:03:06.37	5.140	Iso	..	≤ 32.18	≤ 31.80	11
NGC6517 / $d = 10.6$ kpc (Harris 1996)								
NGC6517 A	18:01:50.61	-08:57:31.85	7.176	Iso	..	≤ 32.06	≤ 31.67	13
NGC6517 C	18:01:50.74	-08:57:32.70	3.739	Iso	..	≤ 32.06	≤ 31.67	13
NGC6517 D	18:01:55.37	-08:57:24.33	4.227	Iso	..	≤ 32.06	≤ 31.67	13
NGC6544 / $d = 3.0$ kpc (Harris 1996)								
NGC6544 A	18:07:20.36	-24:59:52.90	3.059	BW	0.0711	≤ 31.14	≤ 30.75	8
NGC6544 B	18:07:20.87	-25:00:01.92	4.186	Oth	9.957	≤ 31.14	≤ 30.75	8
NGC6626 (M28) / $d = 5.5$ kpc (Harris 1996)								
M28 B	18:24:32.55	-24:52:04.29	6.547	Iso	..	≤ 30.83	≤ 30.52	14
M28 C	18:24:32.19	-24:52:14.66	4.159	Oth	8.078	≤ 30.83	≤ 30.52	14
M28 E	18:24:33.09	-24:52:13.57	5.420	Iso	..	≤ 30.83	≤ 30.52	14
M28 F	18:24:31.81	-24:49:25.03	2.451	Iso	..	≤ 30.83	≤ 30.52	14
M28 J	18:24:32.73	-24:52:10.18	4.039	BW	0.0974	≤ 30.83	≤ 30.52	14
NGC6652 / $d = 10.0$ kpc (Harris 1996)								
NGC6652 A	18:35:44.86	-32:59:25.08	3.889	Iso	..	≤ 31.25	≤ 30.88	15
NGC6656 (M22) / $d = 3.2$ kpc (Harris 1996)								
M22 B	18:36:24.35	-23:54:28.70	3.232	Iso	..	≤ 30.46	≤ 30.08	13
NGC6752 / $d = 4.0$ kpc (Harris 1996)								
NGC6752 E	19:10:52.16	-59:59:02.10	4.572	Iso	..	≤ 29.94	≤ 29.87	16
NGC6760 / $d = 7.4$ kpc (Harris 1996)								
NGC6760 A	19:11:11.09	01:02:09.74	3.619	BW	0.1410	≤ 31.36	≤ 30.97	17
NGC6760 B	19:11:12.57	01:01:50.44	5.384	Iso	..	≤ 31.36	≤ 30.97	17
NGC7099 (M30) / $d = 8.1$ kpc (Harris 1996)								
M30 A	21:40:22.41	-23:10:48.79	11.019	RB	0.1740	≤ 31.07	≤ 30.76	18

Note. Luminosities in column 7 & 8 were calculated by assuming a single power-law model with a fixed $\Gamma=2$.

Ref. (1)Freire et al. (2017) (2) Ridolfi et al. (2016) (3) Ridolfi et al. (2019) (4) Cadelano et al. (2019) (5) Freire et al. (2008b) (6) Pallanca et al. (2014) (7) Wang et al. (2020) (8) Lynch et al. (2012) (9) Ridolfi et al. (2021) (10) Vleeschower et al. (2022) (11) Freire et al. (2008a) (12) Prager et al. (2017) (13) Lynch et al. (2011) (14) Bogdanov et al. (2011) (15) DeCesar et al. (2015) (16) Forestell et al. (2014) (17) Freire et al. (2005) (18) Ransom et al. (2004)

Table 4. Derived parameters of 25 MSPs in GCs with estimates of intrinsic spin-down rate \dot{P}_{int}

MSP Name	P (ms)	\dot{P}_{int} (s/s)	$\log_{10}\dot{E}$ (erg s $^{-1}$)	$\log_{10}B_s$ (G)	Ref.
Correction by long-term radio timing					
47Tuc E	3.536	$(1.2\pm 0.4) \times 10^{-20}$	$34.03^{+0.12}_{-0.16}$	$8.31^{+0.06}_{-0.08}$	1
47Tuc H	3.210	$(9.0\pm 9.0) \times 10^{-21}$	$34.03^{+0.30}_{-34.03}$	$8.23^{+0.15}_{-8.23}$	1
47Tuc J	2.101	$(3.6\pm 2.3) \times 10^{-19}$	$36.19^{+0.22}_{-0.46}$	$8.94^{+0.11}_{-0.23}$	2
47Tuc R	3.480	$(3.1\pm 2.2) \times 10^{-20}$	$34.46^{+0.23}_{-0.54}$	$8.52^{+0.12}_{-0.27}$	1
47Tuc T	7.588	$(9.9\pm 8.9) \times 10^{-20}$	$33.95^{+0.28}_{-1.00}$	$8.94^{+0.14}_{-0.50}$	1
47Tuc U	4.343	$(1.8\pm 0.5) \times 10^{-20}$	$33.94^{+0.11}_{-0.14}$	$8.45^{+0.05}_{-0.07}$	1
47Tuc Y	2.197	$(4.7\pm 3.3) \times 10^{-21}$	$34.24^{+0.23}_{-0.53}$	$8.01^{+0.12}_{-0.26}$	1
Terzan5 ae $^{+}$	3.659	$(3.9\pm 2.6) \times 10^{-19}$	$35.50^{+0.22}_{-0.46}$	$9.08^{+0.11}_{-0.23}$	2
Terzan5 M $^{+}$	3.570	$(1.8\pm 1.1) \times 10^{-20}$	$34.18^{+0.22}_{-0.46}$	$8.40^{+0.11}_{-0.23}$	2
Terzan5 N	8.667	$(1.7\pm 1.1) \times 10^{-19}$	$34.01^{+0.22}_{-0.46}$	$9.08^{+0.11}_{-0.23}$	2
Terzan5 O	1.677	$(1.6\pm 1.0) \times 10^{-19}$	$36.13^{+0.22}_{-0.46}$	$8.72^{+0.11}_{-0.23}$	2
Terzan5 V	2.073	$(3.8\pm 2.5) \times 10^{-20}$	$35.22^{+0.22}_{-0.46}$	$8.45^{+0.11}_{-0.23}$	2
Terzan5 W $^{+}$	4.205	$(1.1\pm 0.7) \times 10^{-19}$	$34.78^{+0.22}_{-0.46}$	$8.84^{+0.11}_{-0.23}$	2
Terzan5 X	2.999	$(2.6\pm 1.7) \times 10^{-20}$	$34.58^{+0.22}_{-0.46}$	$8.45^{+0.11}_{-0.23}$	2
Terzan5 Y $^{+}$	2.048	$(9.5\pm 6.1) \times 10^{-20}$	$35.64^{+0.22}_{-0.46}$	$8.64^{+0.11}_{-0.23}$	2
Terzan5 Z	2.463	$(1.2\pm 0.8) \times 10^{-20}$	$34.49^{+0.22}_{-0.46}$	$8.23^{+0.11}_{-0.23}$	2
Correction by King model					
47Tuc C	5.767	$(2.4^{+5.8}_{-2.4}) \times 10^{-21}$	$32.70^{+0.53}_{-32.70}$	$8.07^{+0.27}_{-8.07}$	3
47Tuc D	5.358	$(2.6^{+1.1}_{-0.8}) \times 10^{-20}$	$33.83^{+0.15}_{-0.16}$	$8.57^{+0.07}_{-0.08}$	3
47Tuc L	4.346	$(2.2^{+3.7}_{-2.2}) \times 10^{-20}$	$34.02^{+0.43}_{-34.02}$	$8.49^{+0.22}_{-8.49}$	3
47Tuc M	3.677	$(4.0\pm 3.0) \times 10^{-21}$	$33.50^{+0.24}_{-0.60}$	$8.08^{+0.12}_{-0.30}$	4
47Tuc N	3.054	$(1.3^{+1.1}_{-0.8}) \times 10^{-20}$	$34.27^{+0.25}_{-0.36}$	$8.31^{+0.13}_{-0.18}$	3
47Tuc O	2.643	$(1.5^{+0.4}_{-0.5}) \times 10^{-20}$	$34.49^{+0.10}_{-0.20}$	$8.29^{+0.05}_{-0.10}$	3
47Tuc Q	4.033	$(3.0\pm 0.2) \times 10^{-20}$	34.26 ± 0.03	8.54 ± 0.01	3
NGC6397 A	3.650	$(1.6\pm 1.2) \times 10^{-19}$	$35.10^{+0.24}_{-0.60}$	$8.88^{+0.12}_{-0.30}$	4
M28 A (MSP with large \dot{P})					
M28 A	3.054	$(1.62\pm 9 \times 10^{-7}) \times 10^{-18}$	$36.35\pm (2 \times 10^{-7})$	$9.35\pm (1 \times 10^{-7})$	5,6

Note. The flag “+” in column 1 indicates the MSPs without X-ray counterparts identified (cf. Table 3).

Ref. (1) Freire et al. (2017) (2) Prager et al. (2017) (3) Bogdanov et al. (2006) (4) Grindlay et al. (2002) / (5) Foster et al. (1988)/ (6) Cognard et al. (1996)

Table 5. The results of Spearman rank test for the correlation between L_x and \dot{E} with the samples of GC MSPs in three different groups (see main text).

	0.3 – 8 keV		2 – 10 keV	
	Spearman'r	p -value	Spearman'r	p -value
Group A	0.692	0.013	0.727	0.007
Group B	0.676	0.001	0.734	2×10^{-4}
Group C	0.721	2×10^{-4}	0.770	4×10^{-5}

Table 6. The results of Spearman rank test for the correlation between P_b and P with radio/X-ray selected MSPs in GCs and GF.

	Radio selected		X-ray selected	
	Spearman'r	p -value	Spearman'r	p -value
GC	0.164	0.126	-0.111	0.512
GF	0.391	7×10^{-9}	0.304	0.060

Table 7. Null hypothesis probabilities of K-S and A-D tests for comparing the X-ray properties between the MSPs in GCs and GF.

	Whole		Iso		Oth		BW		RB	
	K-S	A-D	K-S	A-D	K-S	A-D	K-S	A-D	K-S	A-D
Γ	0.552	0.534	0.053	0.110	0.360	0.344	0.254	0.190	0.929	0.935
L_x^{2-10}	0.033	0.019	0.032	0.077	0.161	0.062	0.227	0.227	0.519	0.433

Table 8. Null hypothesis probabilities of K-S and A-D tests for comparing the physical properties between radio/X-ray selected MSPs in GCs and GF. Both results with the GC MSP samples adopted from Group B and Group C are given in this table.

	GC vs. GF				Radio selected vs. X-ray selected			
	Radio selected		X-ray selected		GC		GF	
	K-S	A-D	K-S	A-D	K-S	A-D	K-S	A-D
P_b	5×10^{-7}	2×10^{-5}	0.464	0.748	0.722	0.710	2×10^{-4}	0.001
P	0.036	0.007	0.013	0.016	0.241	0.125	8×10^{-4}	0.002
B_s (outliers excluded)	0.005	0.002	0.019	0.019	1.0	1.0	0.726	0.622
B_s (outliers included)	0.004	0.001	0.022	0.019	1.0	1.0	0.736	0.673
\dot{E} (outliers excluded)	5×10^{-5}	2×10^{-4}	0.807	0.711	1.0	1.0	1×10^{-5}	1×10^{-4}
\dot{E} (outliers included)	5×10^{-5}	2×10^{-4}	0.715	0.557	1.0	1.0	7×10^{-6}	9×10^{-5}

Table 9. The median for the physical properties between radio/X-ray selected MSPs in GCs and GF. For B_s and \dot{E} , the values inside and outside the parentheses are the medians with the outliers excluded and included respectively.

	GF		GC	
	Radio selected	X-ray selected	Radio selected	X-ray selected
P_b (day)	4.78	0.61	0.79	0.46
P (ms)	3.73	2.95	4.34	3.69
B_s (10^8 G)	1.94 (1.93)	1.91 (1.82)	3.07 (2.95)	2.83 (2.83)
\dot{E} (10^{34} erg/s)	0.49 (0.49)	1.73 (1.63)	1.87 (1.85)	1.82 (1.79)

Table 10. Parameters for various assumed linear models as inferred from Bayesian regression. The best-fit values correspond to the peak values of the marginalized posterior probability distributions. And the uncertainties are estimated from the ranges with 68% of the samples bracketed.

	Slope	Intercept	Slope	Intercept	Slope	Intercept	Slope	Intercept
	GF (outliers excluded)		GF (All)		GC (Group B)		GC (Group C)	
$L_x^{0.3-8} - \dot{E}$	0.86±0.16	1.36±5.36	0.94±0.12	-1.30±4.17	0.36±0.09	18.51±3.19	0.56±0.14	11.43±4.90
$L_x^{2-10} - \dot{E}$	1.03±0.26	-4.92±8.91	1.17±0.23	-9.57±7.77	0.48±0.11	13.70±3.87	0.77±0.18	3.96±6.17
			GF				GC	
$L_x^{0.3-8} - \Gamma$			-0.88±0.17	32.91±0.36			-0.85±0.14	33.06±0.34
$L_x^{2-10} - \Gamma$			-1.49±0.20	33.67±0.41			-1.39±0.15	33.82±0.35
	GF (Radio selected: All)		GF (Radio selected: HeWD only)					
$P_b - P$	0.078±0.017	0.549±0.018	0.064±0.026	0.537±0.032				

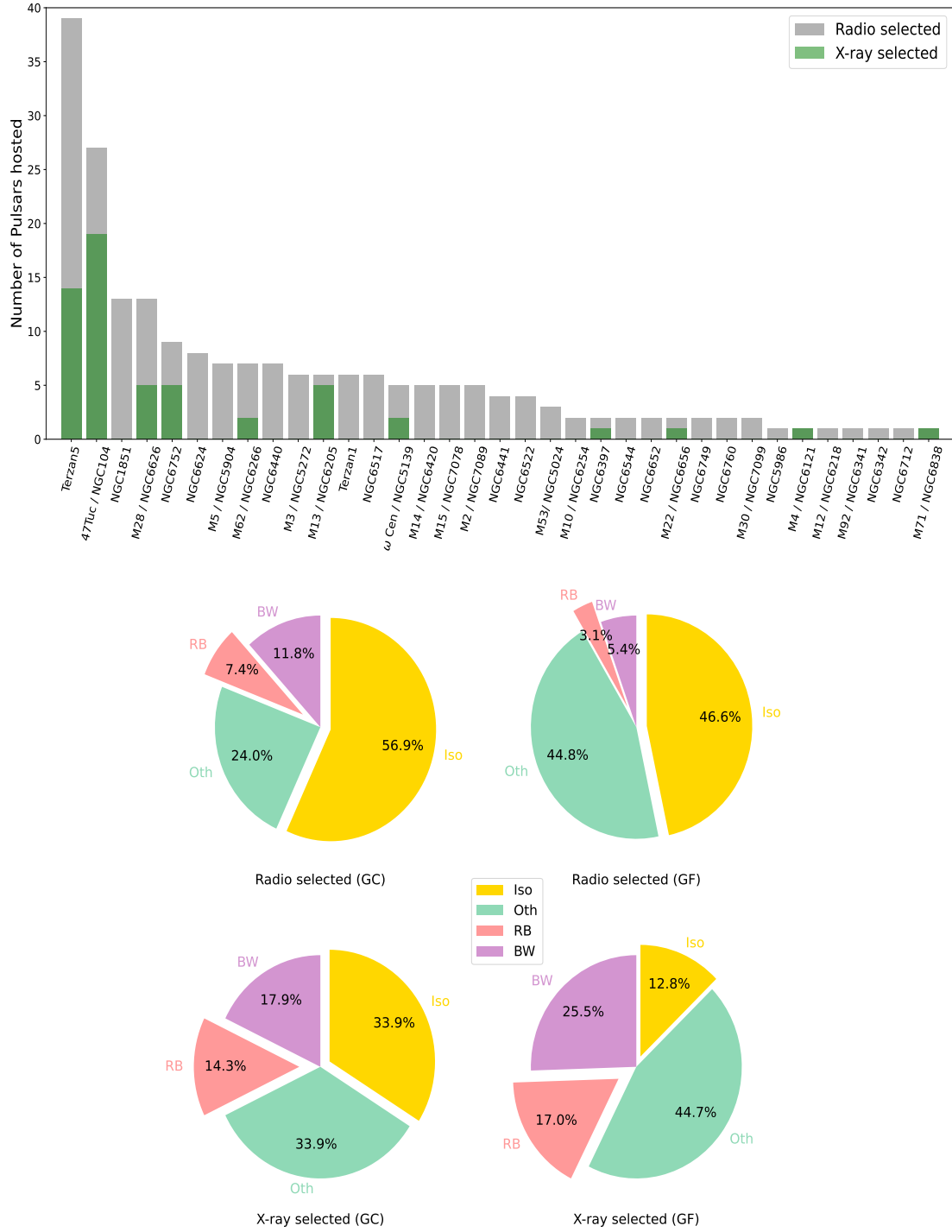


Figure 1. (Upper panel) Updated statistics of X-ray selected and radio selected GC MSPs adopted in this work. (Lower panel) The distributions of different classes of the known radio/X-ray selected MSPs in GCs and GF.

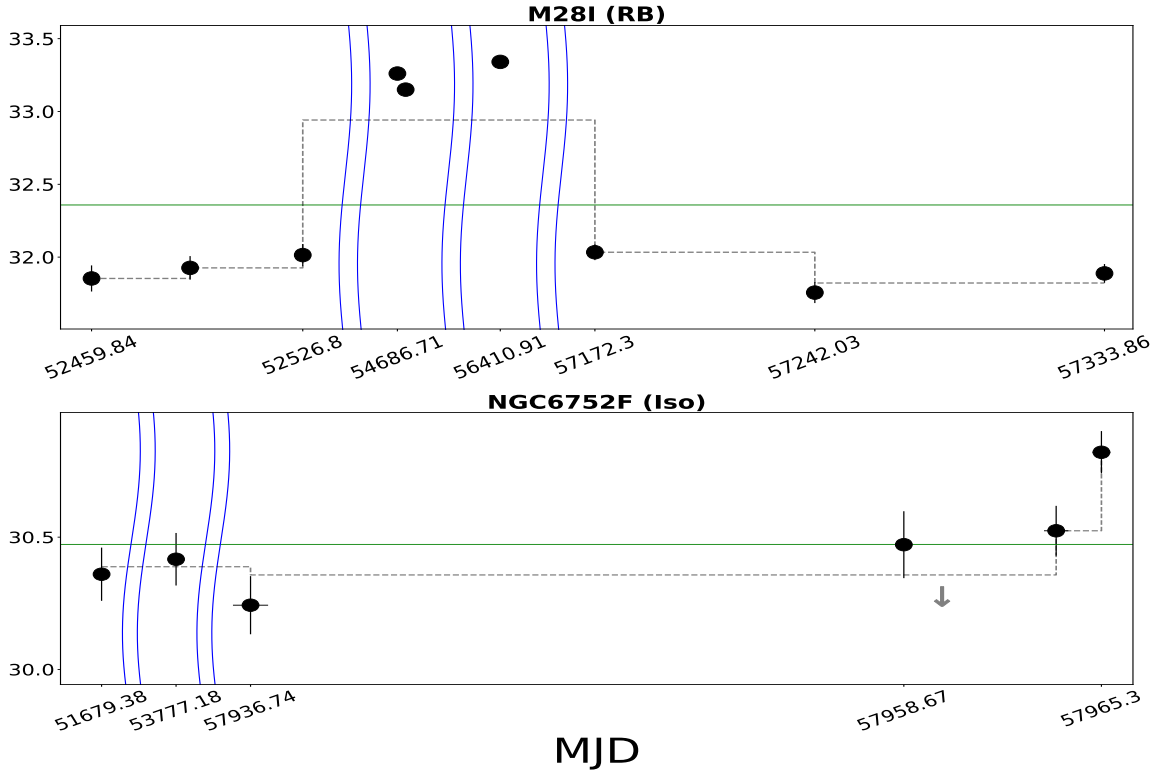


Figure 2. X-ray light curves of the GC MSPs which exhibit long-term flux variability. The Bayesian Block representation of the light curves are illustrated by the dashed lines. The green horizontal lines represent the levels of the mean flux in each case. The time axes are in linear scale with the gaps larger than 1 years intermitted by the blue stripes. The labeled epochs correspond to the midpoints of the observations. The arrow in the plot of NGC6752 F represent the 1σ upper limits of L_x for that particular epoch.

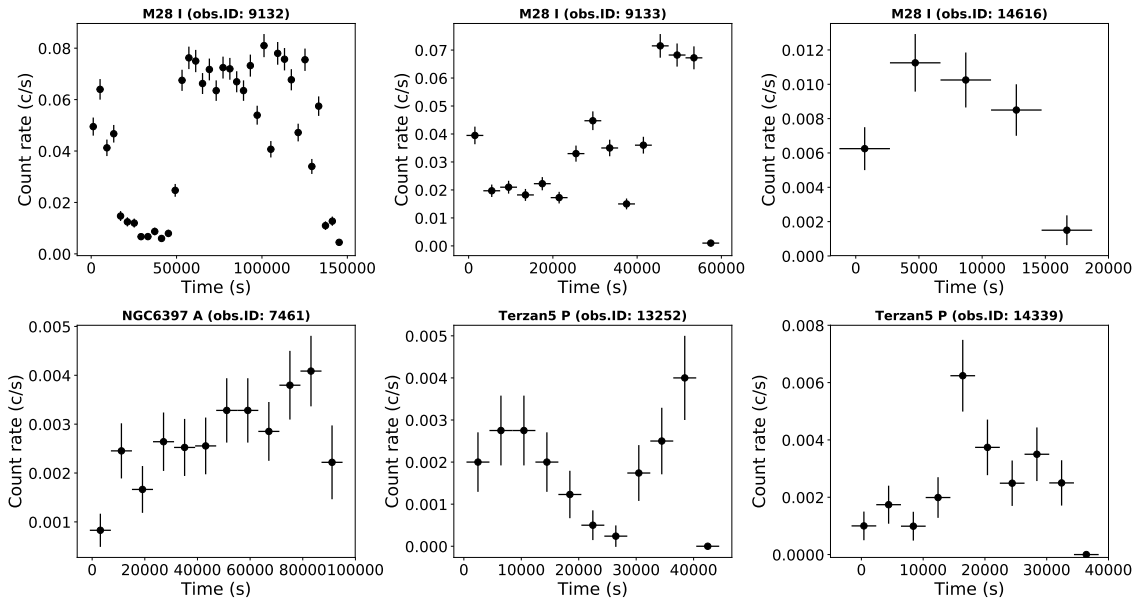


Figure 3. Background-subtracted X-ray light curves of GC MSPs from the individual observations in which short-term variabilities are identified. The optimal binning are determined by CIAO tool `glvary`.

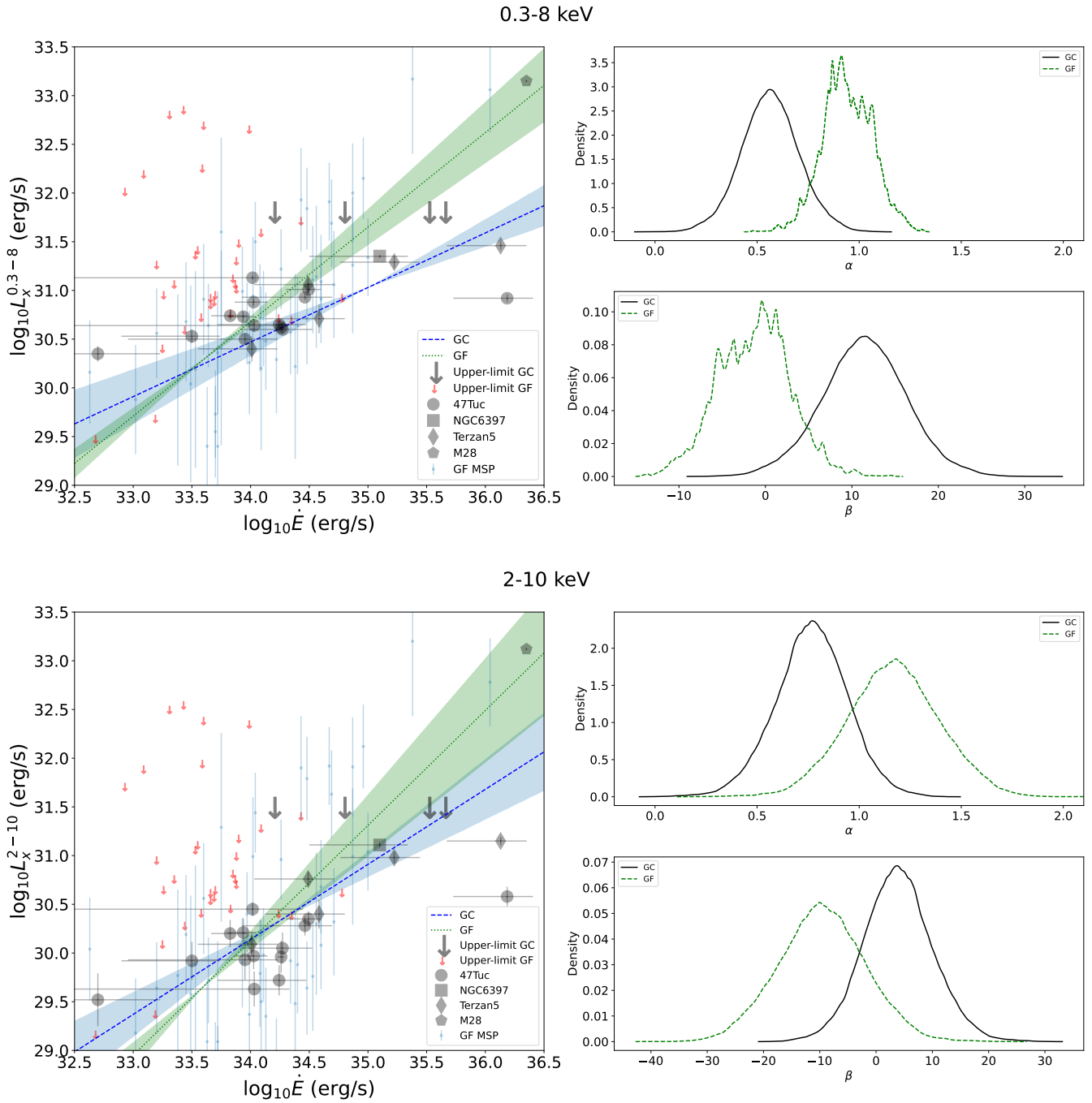


Figure 4. *Upper-left* panel shows the plot of L_x vs. \dot{E} of GC MSPs in 0.3-8 keV for Group C. The blue dashed line and the corresponding shaded region show the best-fit linear model $\log L_x = \alpha \log \dot{E} + \beta$ as inferred from the censored data (i.e. confirmed detection + upper-limits) and the uncertainty respectively (cf. Table 10). The corresponding relation (i.e. green dotted line + shaded region) for the GF MSPs in the same band is plotted for comparison. Samples from different GCs are illustrated by different symbols. *Lower panel* shows the same plot but for the energy band 2-10 keV. Marginalized posterior probability distributions of the model parameters are shown in the *upper-right* and *lower-right* panels for 0.3-8 keV and 2-10 keV respectively.

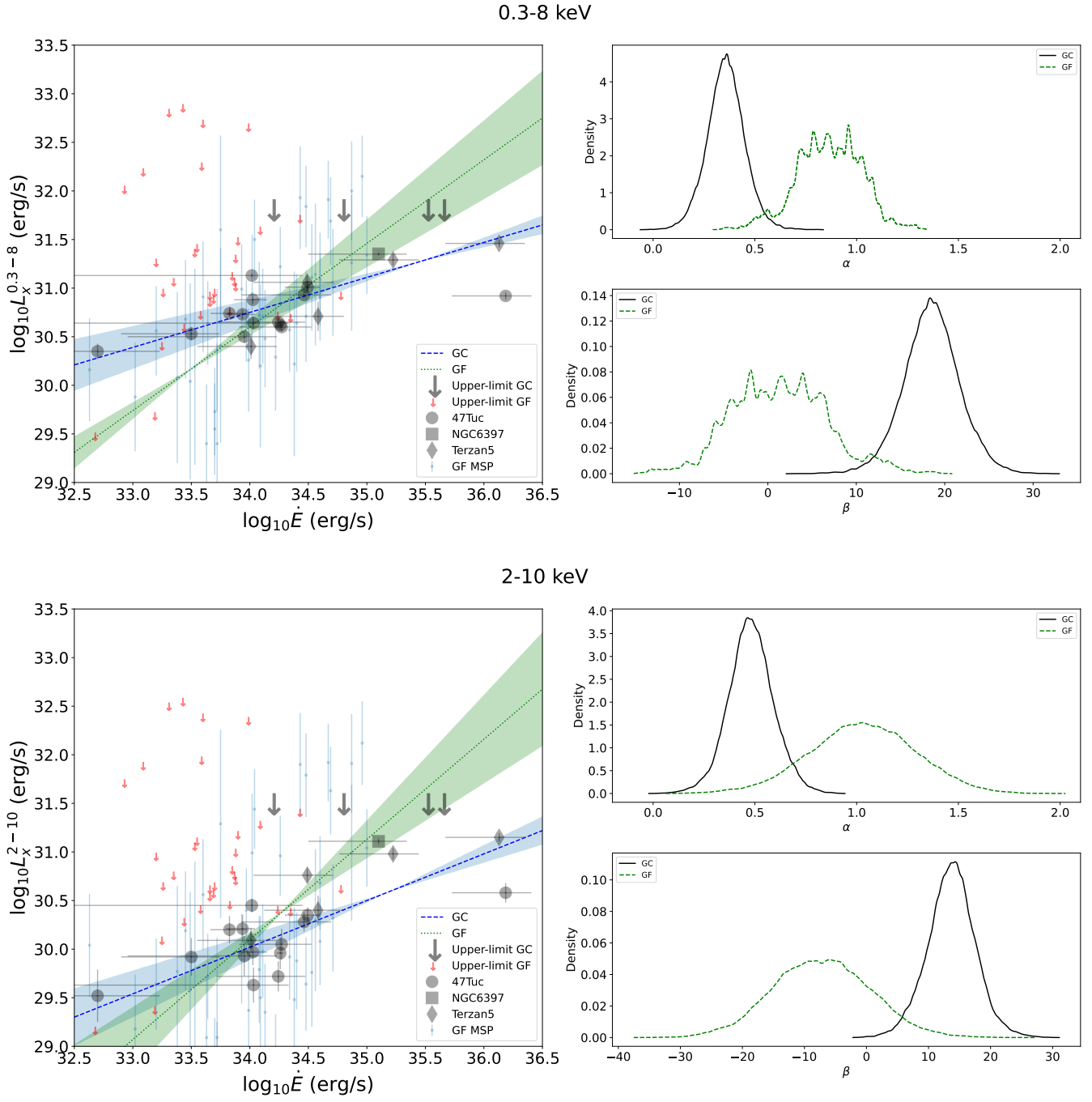


Figure 5. Same as Figure 4 but with the outliers in both GCs (i.e. M28 A) and GF (i.e. PSR J0218+4232 and PSR B1937+21) excluded.

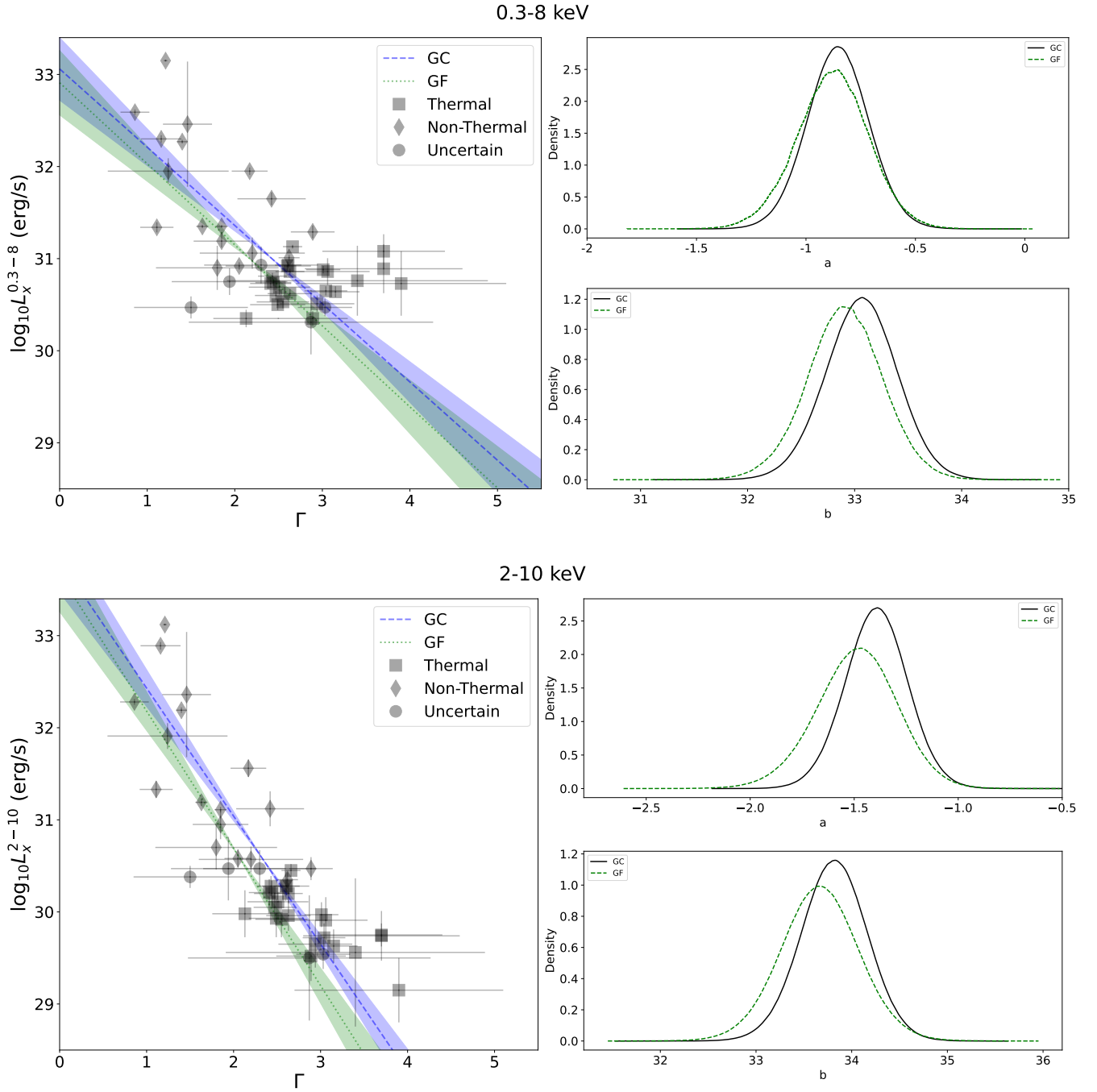


Figure 6. Correlation between L_x and Γ of X-ray detected GC MSPs in 0.3-8 keV (*Upper-left panel*) and 2-10 keV (*Lower-left panel*). The blue dashed line and the corresponding shaded region show the best-fit linear model $\log L_x = a\Gamma + b$ for GC MSPs as well as the uncertainty (cf. [Table 10](#)). The corresponding relation (i.e. green dotted line + shaded region) for the GF MSPs in the same band is plotted for comparison. Marginalized posterior probability distributions of the model parameters are shown in the *upper-right* and *lower-right* panels for 0.3-8 keV and 2-10 keV respectively.

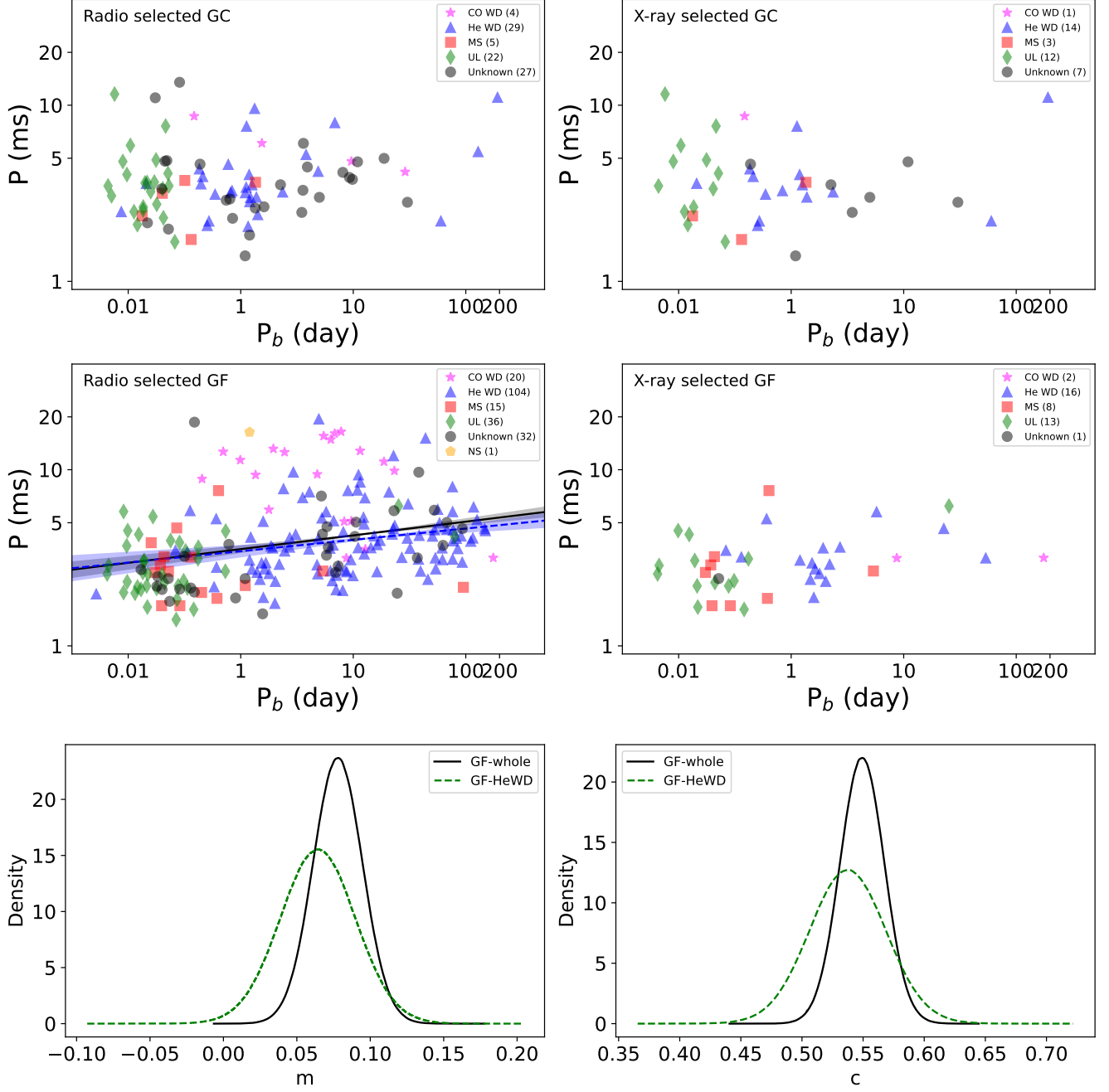


Figure 7. The plots of P_b vs. P of radio/X-ray selected MSP binaries in GCs (*Top left/right panels*) and GF (*Middle left/right panels*). Systems with different companions are represented by different symbols. The bracketed numbers in the legends show the sample sizes in each class. The solid and the dashed lines in the *middle-left panel* represent the best-fit model $\log P = m \log P_b + c$ for the whole radio selected GF MSPs and those with He WD as companions respectively (cf. [Table 10](#)). *Lower-left and lower-right panels* show the marginalized posterior probability distributions for the model parameters.

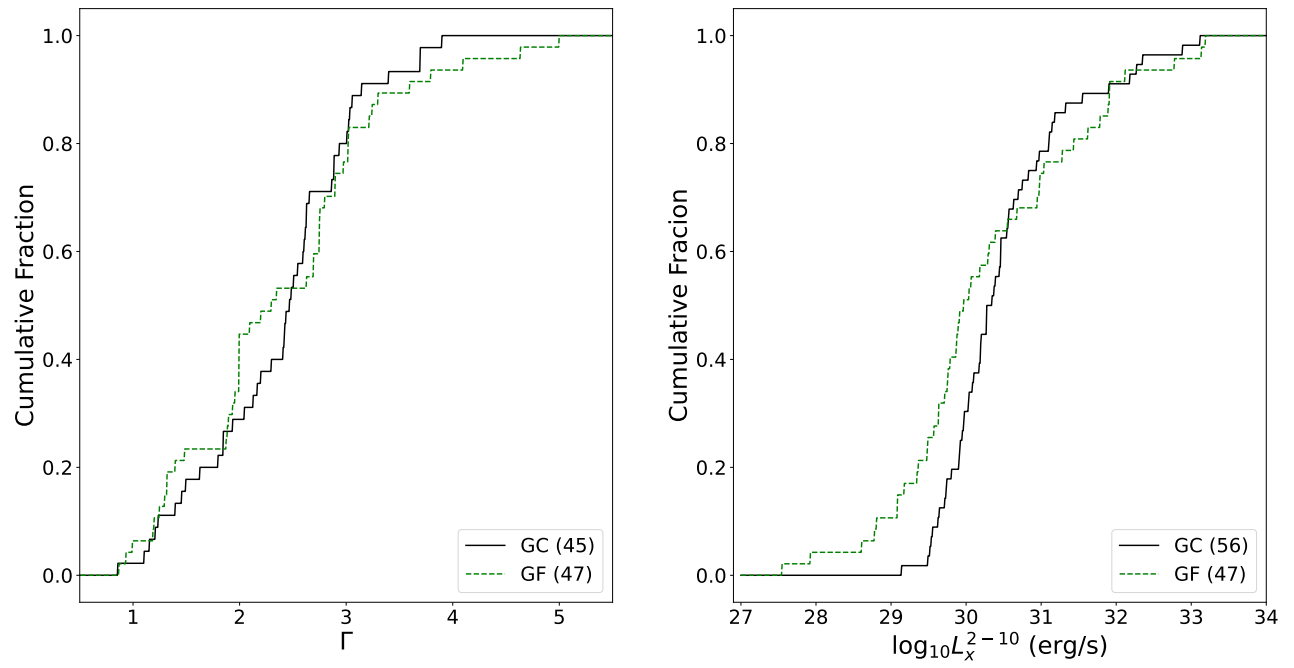
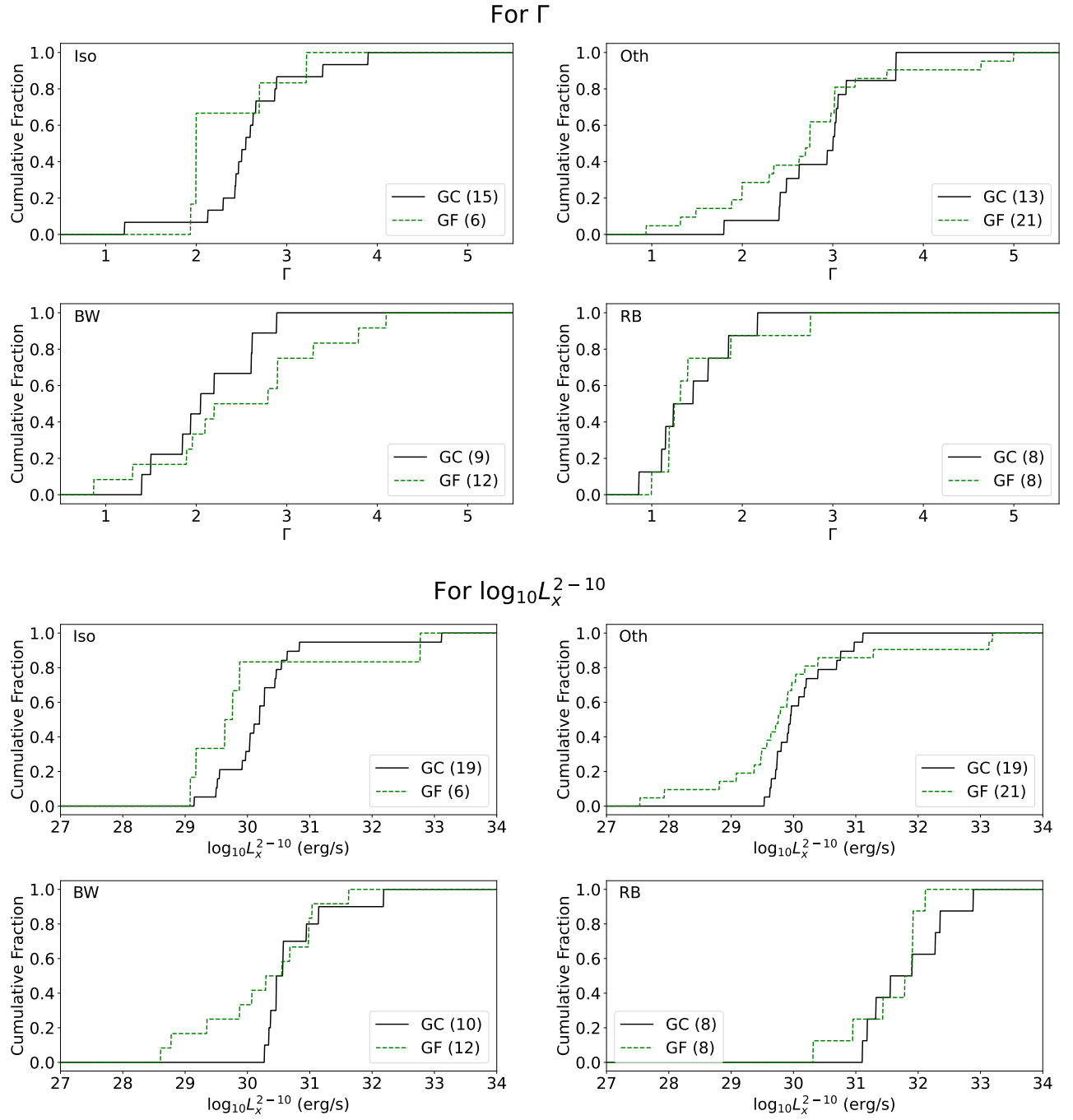


Figure 8. Comparisons of eCDFs of Γ and L_x between GC MSPs and GF MSPs. The bracketed numbers in the legends show the sample sizes.



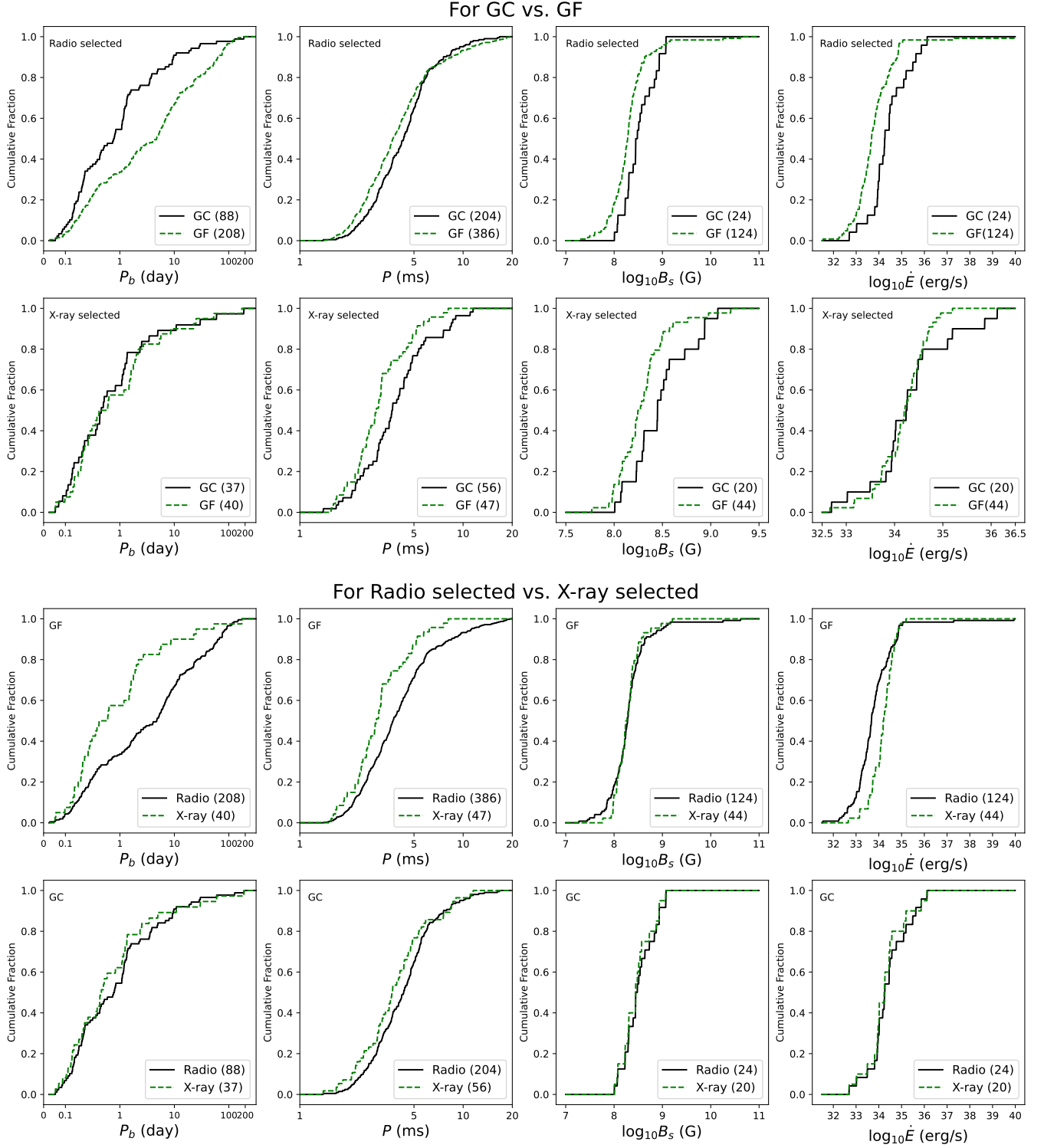


Figure 10. (First row) Comparisons of eCDFs of P_b , P , B_s and \dot{E} between radio selected MSPs in GCs and GF. The outliers in both GCs (i.e. M28 A) and GF (i.e. PSR J0218+4232 and PSR B1937+21) are excluded in comparing B_s and \dot{E} . (Second row) Comparisons of the same set of parameters between X-ray selected MSPs in GCs and GF. (Third row) Comparisons the same set of parameters between X-ray selected and radio selected MSPs in GF. (Fourth row) Comparisons the same set of parameters between X-ray selected and radio selected MSPs in GCs.

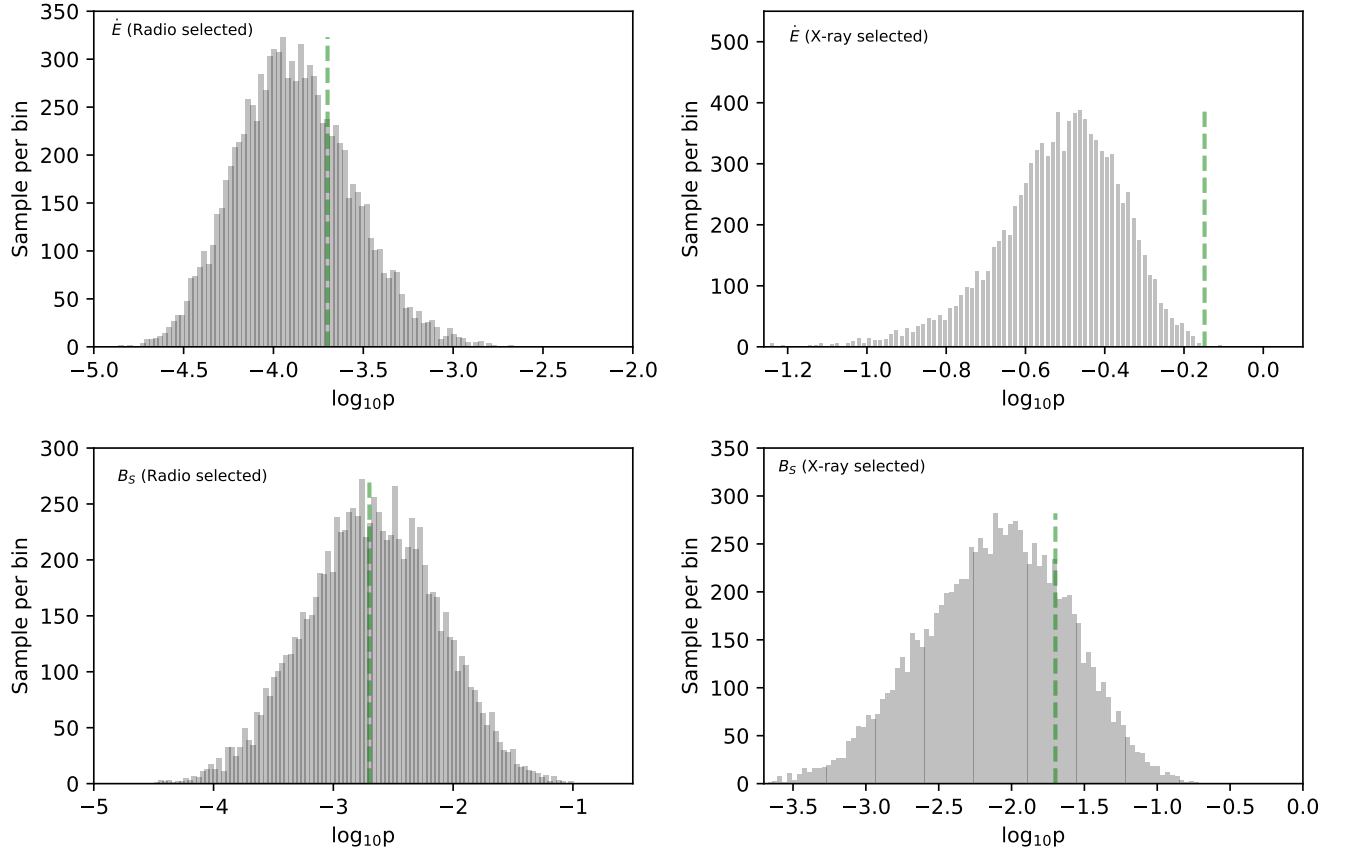


Figure 11. Empirical distributions of null hypothesis probabilities (i.e. p -values) resulted from the A-D test in comparing 10000 sets of simulated samples of \dot{E} and B_s drawn from both GC and GF samples with outliers excluded. The green dashed lines illustrate the p -values obtained from comparing the observed samples between GC and GF.

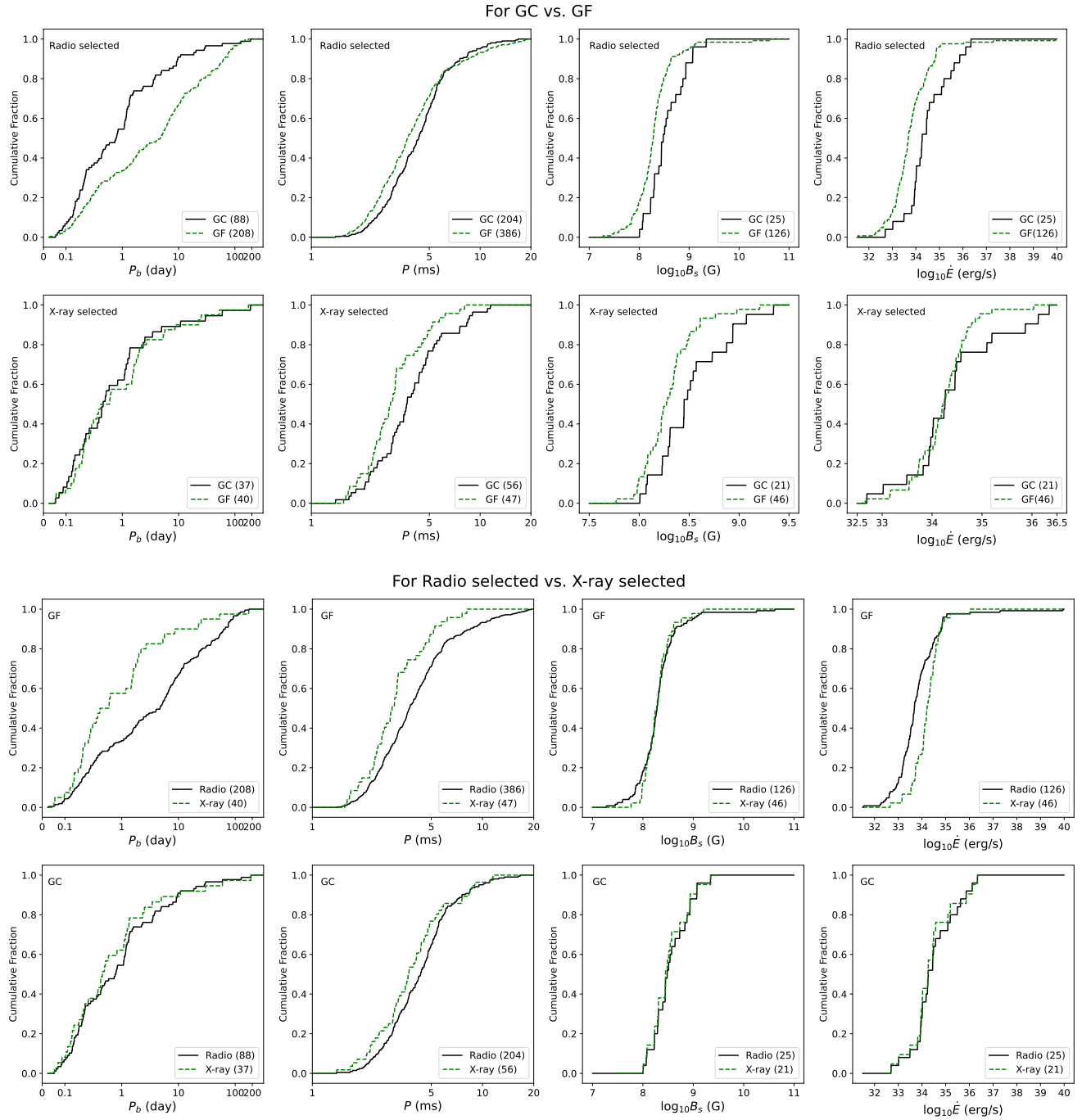


Figure 12. Same as Figure 10 but with M28 A, PSR J0218+4232 and PSR B1937+21 included for comparing B_s and \dot{E} .

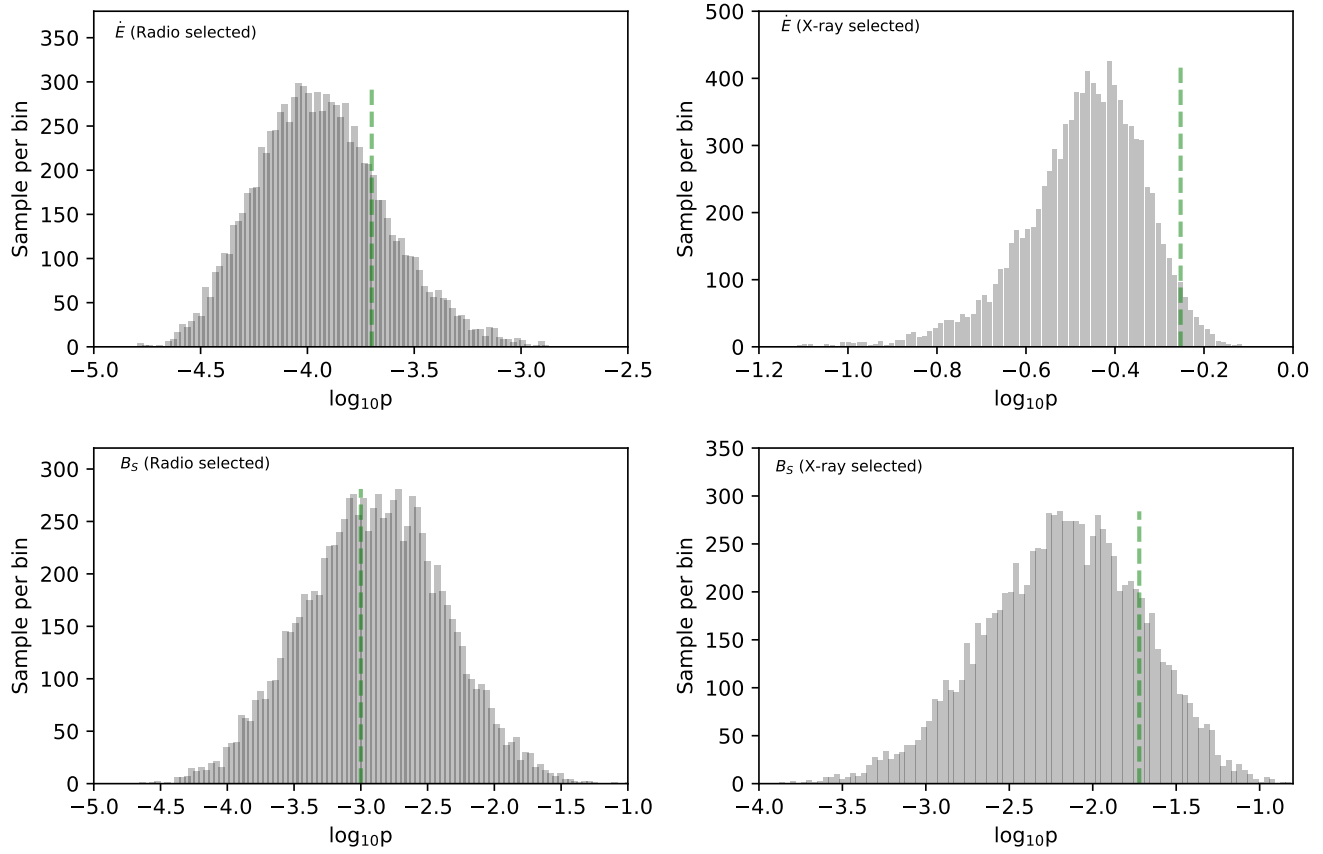


Figure 13. Same as Figure 11 but with M28 A, PSR J0218+4232 and PSR B1937+21 included.